Spring 1973

TEMPERATURE-DEPENDENCE OF THE ELECTRON-SODIUM AND ELECTRON-RUBIDIUM SPIN-EXCHANGE CROSS-SECTIONS

STEVEN JOSEPH DAVIS

TEMPERATURE DEPENDENCE OF THE e-Na AND e-Rb SPIN-EXCHANGE CROSS SECTIONS

by

STEVEN J. DAVIS

B.S., University of New Hampshire, 1969

A THESIS

Submitted to the University of New Hampshire

In Partial Fulfillment of

The Requirements for the Degree of

Doctor of Philosophy

Graduate School

Department of Physics

June, 1973

This thesis has been examined and approved.

L. C. Balling

Thesis director, L. C. Balling, Asso. Prof. of Physics

R. H. Lambert

R. H. Lambert, Prof. of Physics

Lyman Mower

L. Mower, Prof. of Physics

J. J. Wright

J. J. Wright, Asst. Prof. of Physics

John F. Dawson

J. F. Dawson, Asst. Prof. of Physics

May 21, 1973

Date

ACKNOWLEDGMENTS

I wish to express my sincere appreciation to my thesis advisor, Dr. L. C. Balling, for his patient guidance and encouragement throughout the duration of this work, and for his enthusiastic participation in the laboratory. I also wish to thank Dr. R. H. Lambert and Dr. J. J. Wright for many helpful discussions.

I am deeply grateful to my wife, Virginia, for her continual loyal support and encouragement and for her typing of the first draft of this thesis.

Thanks are also to be extended to Mrs. Serene Klumpar and Mrs. Marianne Whitsel for the skillful typing of the final draft of this manuscript.

This work was supported by the National Science Foundation under contracts NSF - GP 9100 and NSF - GP 16814.

TABLE OF CONTENTS

LIST OF TABLES

LIST OF FIGURES

ABSTRACT

TEMPERATURE DEPENDENCE OF THE e-Na

AND e-Rb SPIN-EXCHANGE CROSS SECTIONS

by

STEVEN J. DAVIS

The e-Rb and e-Na spin-exchange cross sections have been measured in a spin-exchange optical pumping experiment as a function of temperature over the range 300-660°K for Rb and 400-725°K for Na. Within experimental error, the cross sections are essentially constant as a function of temperature. Measurements at 293°K give σ_{se} (e-Rb) = (7.0 ± 2.0) x 10^{-14} cm^2 and measurements at 403°K give σ_{se} (e-Na) = (3.2 ± 1.0) x 10^{-14} cm^2.

CHAPTER I

INTRODUCTION

In 1958 Dehmelt[1] performed an experiment which greatly extended the field of optical pumping. In this experiment, free electrons were polarized in a weak magnetic field by undergoing spin exchange collisions with optically pumped Na atoms. Until that time, optical pumping had been used to investigate those few atoms for which suitable resonance lamps were available, i.e. Cs, Hg, K, and Na, although many other atoms could have been studied had lamps been available. Dehmelt's experiment demonstrated that it was possible to orient atoms indirectly by means of spin exchange collisions. In this technique an atom which has been polarized (oriented along a weak magnetic field) by optical pumping undergoes a collision with a second atom and transfers its orientation to the second atom during the collision;

$$A\uparrow + B\downarrow \rightarrow A\downarrow + B\uparrow \ .$$

This eliminated the need for a different resonance lamp for each theoretically "pumpable" element. This was a very significant contribution, as spin exchange optical pumping is experimentally much easier than would be the design, construction, and operation of exotic resonance lamps.

Soon after Dehmelt's paper, spin-exchange optical pumping measurements of several atomic ground states appeared

in the literature. These included the hyperfine ground states of H, D, T,[2-4] N,[5] P,[6] and since then, many more different atoms have been studied.

The experimental extensions rendered by spin-exchange collisions were not limited to atomic energy level measurements. Indeed, Dehmelt, in this initial paper, measured $\frac{g_I(Na)}{g_s(e)}$ an order of magnitude more precisely than previous determinations, and he made an estimation for the Na - e spin-exchange cross section. Spin-exchange has been utilized in many different types of experiments, e.g. measurements of hyperfine pressure and temperature shifts which serve as sensitive tests for theoretical atomic wave functions, measurements of the electron g factor, which test predictions of Q.E.D., determinations of g factor ratios which are of interest as tests for theoretical g factors, and measurements of spin-exchange cross sections for electron-atom and atom-atom collisions which yield information concerning the interaction potentials between the colliding particles.

Interest in spin-exchange is not limited to the realm of optical pumping. In recent years atomic beam workers have measured partial and total spin-exchange cross sections for electron-alkali atom collisions in the eV energy range.[7-8] There is also a great deal of astrophysical interest in spin-exchange cross sections.[9] Astrophysicists measure the hydrogen density both in and beyond our galaxy by measuring the intensity of the 21 cm hydrogen ground

state hyperfine emission line.[10] Since spin-exchange collisions can change the populations of these hyperfine levels, they play an important role in determining the radiative transition rates between the ground state hyperfine levels. Also, the effect of frequency shifts due to H-H spin exchange collisions must be considered in the operation of a hydrogen maser as a frequency standard.[11,12]

Many theoretical investigations concerning electron-alkali atom low energy elastic scattering have been completed in recent years. These calculations have been approached essentially in two different ways. The first is called the "adiabatic" or polarized orbital model. Here, the fact that the collision time (10^{-12}sec)[13] is much greater than the atomic period (10^{-15}sec),[14] is utilized in assuming that the atomic system is able to react, (polarize), in response to the incident electron.[15] The atomic wave functions are thus assumed to change adiabatically during the collision process. Calculations of this type have been carried out on Cs,[15,16] Rb,[17] Li, and Na.[18]

The second method, called close-coupling, assumes the mass of the alkali nucleus to be infinite, and the wave function of the alkali atom-electron system is expanded in eigenstates of the alkali atom. The expansion is truncated to exclude all the alkali continuum and upper lying discrete states.[19] The infinite series expansion is thus reduced to a series involving only a finite number of lower lying discrete states of the alkali

atom. Recent close-coupling calculations have been completed for Cs, K, Na, and Li by Karule.[20] Burke and Taylor investigated Li in 1969,[21] and most recently Norcross, and Moores and Norcross completed theoretical treatments of Li and Na.[22,23]

As a rule, all of the above calculations are in reasonable agreement with recent atomic beam measurements of both spin-exchange and total elastic cross sections in the eV energy range. In different close-coupling calculations there is consistency among the calculated phase shifts. A discrepancy exists between these calculations and previous optical pumping measurements. These differences will be discussed shortly, but first a brief description of spin-exchange optical pumping is necessary.

In these experiments alkali vapor in a cell is oriented along a magnetic field by optical pumping. Electrons, produced by either a continuous rf discharge or the ionizing radiation of tritium gas, undergo spin-exchange collisions with the oriented alkali atoms and themselves become polarized. When an rf magnetic field is tuned to the resonance frequency of the electrons they become depolarized, and through spin-exchange collisions, the alkali atoms become depolarized and absorb some of the pumping light. Experimental conditions can be adjusted so that the electron resonance linewidth is dominated by spin-exchange relaxation. The electron-alkali spin-

exchange collisions also give rise to a shift in the peak of the electron resonance line.[24]

Measurements by Balling and Pipkin[25] for e-Cs collisions gave a much larger spin-exchange cross section and much smaller frequency shifts than predicted by Stone and Reitz.[15] Na measurements by Dehmelt,[1] and by Balling[26] yielded a cross section three times greater than predicted by Karule,[20] and Norcross.[22] Similarly, data of e-Rb[24] collisions gave a much smaller shift to broadening ratio than predicted by Bender.[27] These earlier optical pumping studies of the e-alkali atom scattering process were limited to a very narrow temperature range for each alkali species.

This limitation was greatly reduced by the introduction of the high temperature optical pumping technique by Balling, Lambert, Wright, and Weiss[28] in 1969. This method greatly extended the temperature range of optical pumping, opening the door to many experiments, including ground state hyperfine studies of numerous atomic species. The hyperfine ground states and pressure shifts of Li ,[29] N,[30] and Mn[31] have been studied using this technique. The Mn measurements are reported in the appendices of this paper as an example of the utility of spin-exchange optical pumping.

The goal of this experiment, then, was to utilize the high temperature technique to measure the temperature dependence of the e-Rb and the e-Na spin-exchange cross

sections. These measurements would serve as tests for the latest e-Na theory, and also would check the previous e-Na and e-Rb measurements which were made over very limited temperature spans. Calculations of the e-Rb process are within present theoretical means, so e-Rb measurements were also of interest. Since Rb optical pumping is easier than that of sodium, it seemed reasonable to develop the experimental procedure with the e-Rb experiments. Also as shown in the next chapter, the spin-exchange cross section and the frequency shift are both functions of the singlet and triplet scattering phase shifts, hence measurements of these two quantities can yield information about the scattering potentials. Thus measurements of the frequency shifts were also sought.

The high temperature technique which made the measurements proposed above possible, consists of containing the alkali metal in a small sidearm of the sample. The temperature of this sidearm is independently controlled from that of the cell by the continuous flow of a stream of cool air around the tip. This allows the cell to be heated to several hundred degrees C and still keep the alkali density in the cell low enough to afford good optical pumping signals (if the alkali density gets too large, the cell becomes opaque to the pumping light, hence no signal can be seen).

As stated earlier, a separate experiment measuring the ground state of Mn is also reported in this work.

The Mn measurements clearly show the versatility of both the spin-exchange and high temperature techniques.

The next chapter contains a brief description of the optical pumping process, the spin-exchange process, and other theoretical considerations necessary for an understanding of the experiment.

CHAPTER II

THEORY

1. Optical Pumping

Optical pumping is a process in which light is used to alter the relative populations of a set of energy levels of an atomic system from their normal Boltzmann distribution. The following is a brief description of optical pumping as it applies to sodium.

Na has a nuclear spin of I = 3/2 and an electronic ground state of $^2S_{\frac{1}{2}}$.[32] The nuclear spin $\vec{I}$ and electronic angular momentum $\vec{J}$ couple through the hyperfine interaction to form a resultant total atomic angular momentum $\vec{F}$. The possible values of F range in integral steps from $|I - J|$ to I + J. Thus, in the ground state, sodium has a hyperfine doublet; F = 2, F = 1. Each F level has 2 F + 1 magnetic sublevels associated with it, labelled M. M values range in integral steps from F to -F.[33] There are therefore eight substates in the ground state of sodium: (2,2), (2,1), (2,0), (2,-1), (2,-2), (1,1), (1,0), and (1,-1) where the labelling scheme is (F,M).

If a cell containing sodium vapor is placed in a weak, axial magnetic field $H_o\hat{k}$ and illuminated with left circularly polarized D-1 resonance light (5896 Å)[34] incident along the direction of the static field, the

following will happen. Some atoms in sublevels of the ground state will absorb the radiation with the selection rule $\Delta M = +1$ and arrive in the $P_{\frac{1}{2}}$ state. Atoms in the sublevel (2,2) of the ground state, however, cannot absorb the pumping light because there is no sublevel $M = 3$ in the $P_{\frac{1}{2}}$ state. Atoms pumped to the $P_{\frac{1}{2}}$ state spontaneously decay in about 10^{-8} sec.[35] to some sublevel of the ground state with the selection rule $\Delta M = \pm 1,0$. Thus, some atoms end up in the (2,2) sublevel and can no longer absorb light. Ideally the atoms in the (2,2) sublevel would remain there indefinitely since the spontaneous decay rate to a lower sublevel is extremely small. One expects that under the influence of the pumping light all the atoms would be pumped to the (2,2) sublevel, thus obtaining complete orientation of the vapor. However, collisions with the cell walls cause non-radiative transitions which remove atoms from the (2,2) sublevel. To prevent rapid diffusion to the walls, the cells usually contain a few Torr of an inert gas such as Ne or He. Collisions between ground state ($S_{\frac{1}{2}}$) oriented sodium atoms and inert gas atoms have very low disorientation cross sections so the polarization is preserved during collisions.[36] Since the inert gas slows the diffusion of the sodium atoms to the walls by non-disorienting collisions, it is referred to as a buffer gas.

When an rf magnetic field is applied perpendicular to the static field, at the sodium ground state hyperfine or Zeeman frequency, the atoms undergo the appropriate

transitions and the cell becomes depolarized. This is detected by monitoring the transmitted pumping light with a photocell. A partially oriented vapor is partially transparent to the pumping light. However, when the vapor becomes depolarized under the influence of the rf, the atoms absorb the light and the transmitted intensity drops. The signal corresponds to the changes in the transmitted pumping light intensity.

The polarization of the excited $P_{\frac{1}{2}}$ state is a strong function of the amount of buffer gas in the cell, as P state electron - buffer gas collisions have relatively large disorientation cross sections.[37] If the buffer gas pressure is more than $\sim$ 10 Torr,[38] complete reorientation in the excited state is expected. This means that the P state sublevels become equally populated before reemission to the ground state. For this situation the probabilities to return to any ground state sublevel are all equal.[39] The other extreme, no buffer gas, yields no excited state reorientation and the transition probabilities to the ground sublevels are not all equal.

The pumping process for Na which applies equally well for Rb^{87} (I = 3/2) has been examined by Franzen and Emslie[40] for pumping with left circularly polarized D-1 light. The rate equation for the occupation probability of the k^{th} substate is written

$$\dot{P}_k = -\sum_{j=1}^{8}{}' (b_{kj} + w_{kj}) P_k + \sum_{i=1}^{8}{}' (b_{ik} + w_{ik}) P_i ,$$

$$k = 1, 2, \cdots 8 ,$$

where $b_{ij} = \frac{\text{probability}}{\text{unit time}}$ that an atom undergoes a transition from ground substate i to ground substate j via the absorption of a photon and subsequent spontaneous emission, and w_{ij} is the comparable transition rate caused by some relaxation mechanism such as cell walls.

The prime summation means that the j = k and i = k terms are omitted. This is the statement that an atom that undergoes a transition out of the substate k and subsequently returns to the same substate k does not affect the population of that state.

Franzen and Emslie obtain numerical solutions to this set of equations for two limiting cases: 1) complete reorientation in the excited state and 2) no reorientation in the excited state. In both limits the results are roughly the same, i.e. under the influence of the pumping light the occupation probability of the (2,2) sublevel of the ground state approaches a maximum value while the occupation probabilities of all the other ground state sublevels approach zero. This means that the (2,2) sublevel becomes populated at the expense of the other sublevels. This effect in which weakly absorbing levels are populated while the strongly absorbing states are depleted is called depopulation pumping. [41]

It is instructive to look at the pumping process for a fictitious zero nuclear spin alkali atom. The ground state has two sublevels, $|+\rangle$ and $|-\rangle$. We define the respective occupation probabilities as n_+ and n_-. The pumping light, incident along the static magnetic field $H_o\hat{k}$, is assumed left

circularly polarized, hence causes $\Delta M = +1$ transitions. We write the rate equations for n_+ and n_-,

$$\frac{dn_+}{dt} = -P_- n_+ + P_+ n_-,$$

and

$$\frac{dn_-}{dt} = -P_+ n_- + P_- n_+,$$

where $P_- = \frac{\text{probability}}{\text{unit time}}$ that an atom undergoes a transition out of sublevel $|+\rangle$, and $P_+ = \frac{\text{probability}}{\text{unit time}}$ that an atom arrives in the $|+\rangle$ sublevel.

A straightforward solution to this set of equations gives

$$n_+(t) = n_+(0) + \frac{P_+ n_-(0) - P_- n_+(0)}{P_+ + P_-}\left[1 - e^{-(P_+ + P_-)t}\right],$$

$$n_-(t) = n_-(0) - \frac{P_+ n_-(0) - P_- n_+(0)}{P_+ + P_-}\left[1 - e^{-(P_+ + P_-)t}\right].$$

The relative populations of the two levels at t = 0 is given by

$$\frac{n_+(0)}{n_-(0)} = e^{-\frac{(E_+ - E_-)}{kT}}.$$

At room temperatures $\frac{E_+ - E_-}{kT} \approx 0$, so $n_+(0) = n_-(0)$. Now we define the following constants.

$$\alpha \equiv \frac{P_+ n_-(0) - P_- n_+(0)}{P_+ + P_-},$$

$$\beta \equiv P_+ + P_-.$$

We now write the solutions as

$$n_+(t) = n_+(0) + \alpha\left[1 - e^{-\beta t}\right],$$

$$n_-(t) = n_+(0) - \alpha\left[1 - e^{-\beta t}\right].$$

From here we see that if P+ > P-, i.e. pumping is more efficient than relaxation then $\alpha > 0$, which means that n_+ gets greater in time while n_- is reduced. This means that the state $|+\rangle$ becomes populated at the expense of $|-\rangle$, hence the Boltzmann distribution is destroyed.

In the present experiment the linearly oscillating rf field was chopped at 10 Hz in order to utilize a lock-in detector. With the rf set at the appropriate alkali atom Zeeman frequency both the detected optical pumping signal and the chopped rf can be displayed in phase on a dual-trace oscilloscope. An illustration of a typical signal is displayed in figure 1. (The trace of the optical pumping signal is inverted so that absorption increases up along the vertical axis.) During the time interval a b, the rf was off and the cell became pumped, i.e. the alkali vapor gained a macroscopic magnetization along the direction of the static field $H_o\hat{k}$, and the cell became more transparent to the pumping light. At time b the rf was abruptly switched on and the decaying sinewave resulted. At c the rf was shut off and pumping began again. Since the sinewave or "wiggles" were utilized in the data reduction of this work, it seems appropriate to examine them briefly.

For brevity let us assume that the alkali atom

FIGURE 1.

SCOPE TRACING OF

OPTICAL PUMPING SIGNAL

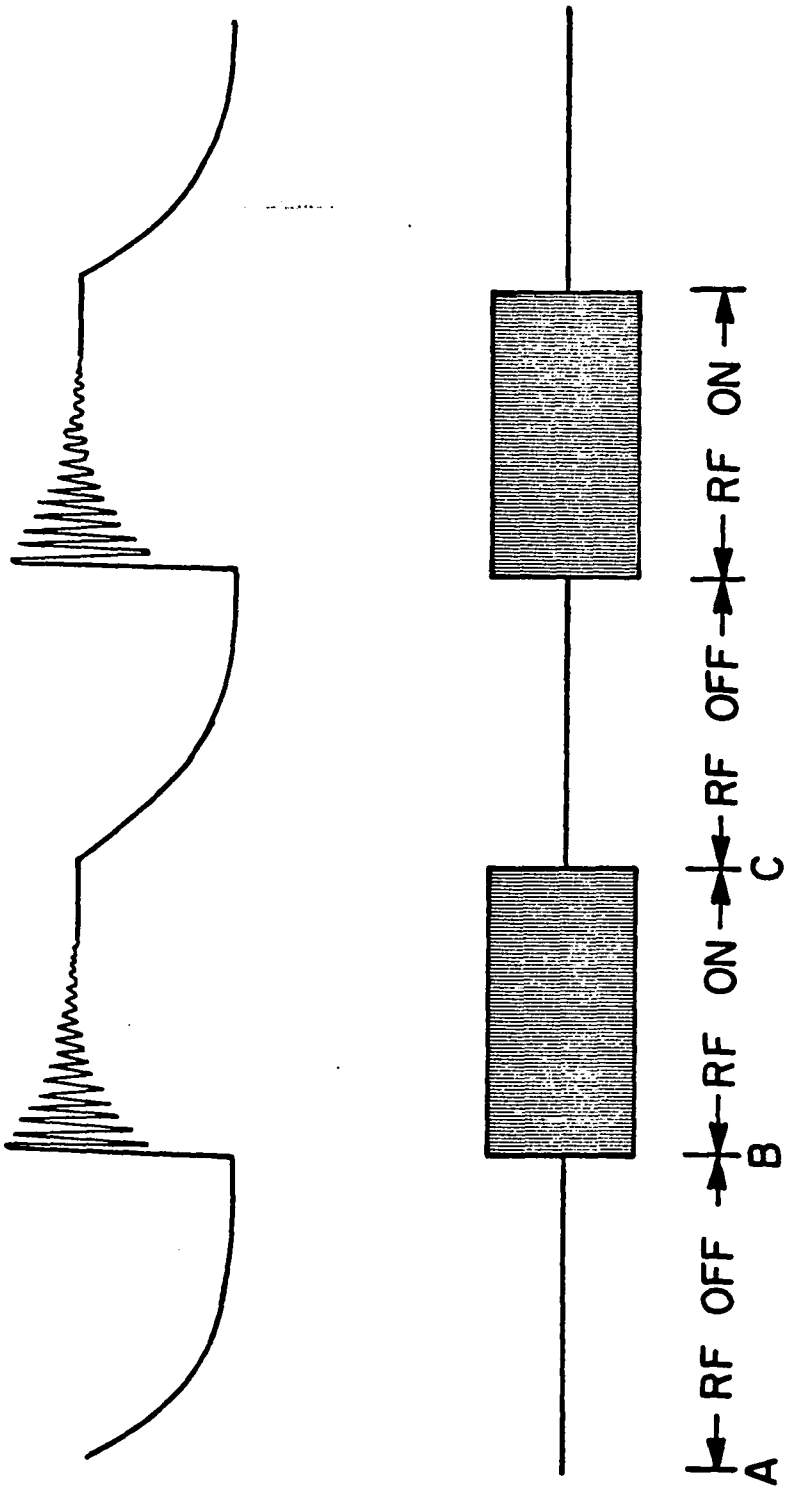
RF OFF
A
RF ON
B
RF OFF
C
RF ON

ground state has only two sublevels, $|+\rangle$ and $|-\rangle$. When σ_+ radiation is applied, pumping takes place. When the sample is pumped then most of the spins "precess" around the static field $H_0\hat{k}$ in the state $|+\rangle$, at frequency ω_0. The effect of the application of the rf is easiest to see in a rotating frame. The linearly oscillating field, $2H_1\hat{\imath}\cos\omega t$, can be written as the superposition of two counter-rotating fields, one rotates in the same direction as the precessing atoms, and one rotates in the opposite direction. If $H_1 << H_0$ then we can neglect the counter-rotating term.[42]

In the rotating (primed) frame the axial field becomes, $\left(H_0 + \frac{\omega}{\gamma}\right)\hat{k}$ where $\vec{\mathcal{M}} = \gamma\vec{J}$ Here $\vec{J}$ is the ground state angular momentum of the atom, and $\vec{\mathcal{M}}$ is the associated magnetic moment. Also, in the rotating frame the rf field is static and equal to $H_1\hat{\imath}$. The fields in the rotating frame are shown in figure 2. The total effective static field in the rotating frame is called H_{eff}. When the rf is off, the atoms precess around H_{eff} which is then in direction $\hat{k}$. If the cell is pumped then most of the spins are in the $|+\rangle$ state thus giving the cell a macroscopic magnetization M_z. When the rf is suddenly turned on at resonance then

$$\left(H_0 + \frac{\omega}{\gamma}\right) = 0,$$

and

$$H_{eff} = H_1 .$$

FIGURE 2

FIELDS IN ROTATING FRAME

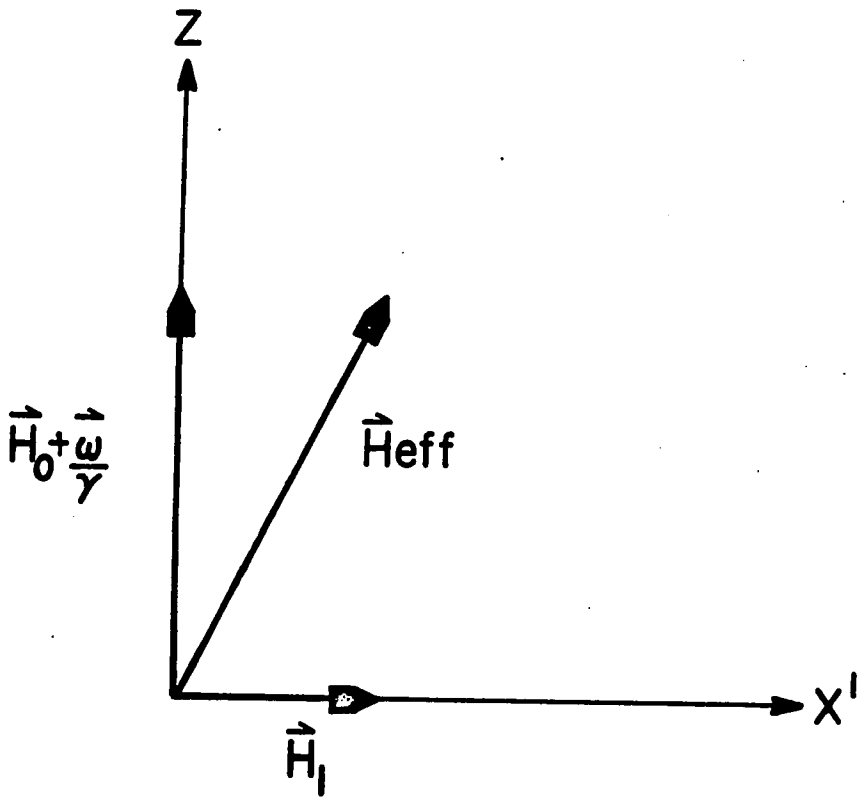
Z
$\vec{H}_0+\frac{\vec{\omega}}{\gamma}$
$\vec{H}_{eff}$
X'
$\vec{H}_1$

The atoms will begin to precess around H_1 and since most were initially up along the z axis, the atoms will precess around H_1 in phase. The coherence of the precessing atoms manifests itself in the precession around H_1 of a macroscopic magnetization M_z. As the phases of the atoms become randomized through collisions and other mechanisms, time variations in the observed M_z disappear. Since the rf rotates around the z axis, observations along the z axis are the same in both frames. In this experiment all optical pumping signals were detected along the z axis, i.e. they were longitudinal.

The signal can now be qualitatively explained. When the rf is turned on, a damped sinusoidal signal appears. This corresponds to the in phase precession of the atoms around the H_1 in the rotating frame. As M_z becomes anti-parallel to $H_o\hat{k}$ (most of the atoms in the $|-\rangle$ state) the atoms can absorb pumping radiation, thus the cell becomes less transparent. Similarly, when the macroscopic magnetization M_z again becomes parallel (most atoms in the $|+\rangle$ state) most atoms cannot absorb light and the cell is more transparent. As the coherence of the spins diminishes (the precessions of the spins around H_1 become random), the wiggles damp away.

Note that if the rf is at the Zeeman frequency then the frequency of the wiggles is determined by H_1, since H_1 is the only field then present in the rotating frame. That is

$$\omega_1 = H_1 \gamma .$$

Thus a measure of the wiggle frequency determines the strength H_1. This was utilized throughout this experiment.

2. Spin-Exchange

The spin-exchange process will now be briefly discussed. The physical origin of spin-exchange and past theoretical treatments are mentioned. Finally a particular treatment of the process is outlined and the steps are traced leading to a predicted optical pumping spin-exchange signal.

Since the actual electron-alkali atom spin-exchange collision is an interaction between the incident electron and the valence electron, we can look at the case of two spin 1/2 particles. The spin dependence of the collision originates in the Pauli exclusion principle.[43] The valence electron and the colliding free electron are indistinguishable. As shown in appendix I the spin-space wave function of the electrons approaching each other with their spins in opposite directions can be expressed as a superposition of singlet and triplet states:

$$\alpha_1 \beta_2 = \frac{1}{\sqrt{2}} \left(\chi_3^0 + \chi_1^0 \right)$$

In appendix I it is also shown that if two identical spin 1/2 particles approach each other in this $\alpha_1 \beta_2$ state, then there is a probability that the final state, after an elastic collision, will be

$$\beta_1 \alpha_2 = \frac{1}{\sqrt{2}} \left(\chi_3^0 - \chi_1^0 \right),$$

which represents a spin flip.

Early theoretical investigations of spin-exchange collisions were done by Purcell and Field,[9] and Dicke and Wittke.[44] Both these calculations were essentially the same. It was assumed that the interacting particles followed classical paths. The mechanism assumed for the exchange process was that the two electron spins, $\vec{S}_1$ and $\vec{S}_2$, rotated about the conserved total $\vec{S}$ during the interaction. Using "semi-classical" arguments, i.e. by assuming spin-exchange only occurs for certain impact parameters, Wittke and Dicke calculated a spin exchange cross section of

$$\sigma_{SE} \sim 2.3 \times 10^{-15} \text{ cm}^2,$$

for H-H spin exchange collisions.

The second method of approach is a partial wave analysis which was first done by Dalgarno.[45] He calculated the triplet and singlet l wave phase shifts δ_l^3 and δ_l^1 and in terms of these phase shifts showed

$$\sigma_{SE} = \frac{\pi}{k^2} \sum_{l=0}^{\infty} (2l+1) \sin^2(\delta_l^3 - \delta_l^1),$$

where $\vec{k}$ is the relative particle momenta divided by $\hbar$. Grossetete has presented a very elegant treatment of spin-exchange relaxation using the density matrix.[13] A partial wave analysis was completed by Balling, Hanson, and Pipkin(BHP), in 1964.[24] This work was performed by density matrix techniques. Since many of the equations of the present experiment were defined in B H P and since it offers some insight into the various parameters of the spin-exchange optical

pumping experiment, some of the steps in their calculations are outlined below.

The model adopted is the following. A cylindrical optical pumping cell of length z_o is considered to be in a weak axial magnetic field, $H_o\hat{k}$. The cell is assumed to contain fictitious nuclear spin zero alkali metal vapor and free electrons. The cell is further assumed to be undergoing the combined effects of pumping radiation and a transverse rf magnetic field at or near the resonant frequency of the electrons. The scattering problem is handled in the center of mass system and the coordinates used are those of the electron relative to the alkali atom.

The nuclear spin = 0 model assumes that nuclear spin effects for electron alkali-atom spin-exchange collisions are unimportant. This assumption also leads to only two ground state sublevels. These are labelled 1 for spin up and 2 for spin down. It is also assumed that there is no coherence introduced by the rf field between these two levels. This is quite reasonable in light of the fact that the rf is not applied at the resonance frequency of the alkali magnetic Zeeman levels. A further justification for this assumption is that the alkali "wiggles" discussed earlier which signal the presence of such coherence are not present in spin-exchange signals. With these assumptions in mind the alkali atom density matrix is written

$$\rho(A) = \begin{pmatrix} \rho_{11}(A) & 0 \\ 0 & \rho_{22}(A) \end{pmatrix},$$

where the zeros imply no "Zeeman coherence." The electron spin-space density matrix is written

$$\rho(e) = \begin{pmatrix} \rho_{11}(e) & \rho_{12}(e) \\ \rho_{21}(e) & \rho_{22}(e) \end{pmatrix} .$$

Here the possibility of coherence between the two electron spin states is accounted for.

It was pointed out earlier that when the rf is tuned to the resonance frequency of the electrons, the transmitted pumping light drops. The difference between the transmitted light for the two cases of rf on and rf off is the quantity that is detected as the signal. As is shown in appendix III, the difference δI_T can be expressed as a function of the corresponding change in the alkali polarization

$$\delta I_T = \frac{N_A Z_o A}{\tau_p} \langle \delta P(A) \rangle ,$$

where Z_o is the length of the cylindrical cell, A is the cross sectional area of the cell, and τ_p is the optical pumping time, i.e. the relaxation time of the alkali vapor under the influence of the pumping light. The brackets indicate that an average has been taken over the length of the cell. The problem of calculating the signal, δI_T, then is one of computing $\langle \delta P(A) \rangle$.

The Z-averaged alkali atom polarization $\langle P(A) \rangle$ will be a function of spin-exchange collisions, disorienting collisions with buffer gas atoms and walls of the cell,

applied rf, and pumping light intensity. The method of calculation involves the computation of the responses of $P(e)$ and $P(A)$ to these parameters. The polarizations are then found by utilizing

$$\langle P(e) \rangle = \langle \rho_{11}(e) \rangle - \langle \rho_{22}(e) \rangle ,$$

and

$$\langle P(A) \rangle = \langle \rho_{11}(A) \rangle - \langle \rho_{22}(A) \rangle .$$

The computational steps leading to an expression for the observed signal are detailed in B H P. The following is not intended to lead the reader step by step, but is only meant as an outline of the key assumptions involved as well as a statement of the results.

The effects of spin-exchange collisions are computed by utilizing the fact that the composite electron-alkali atom density matrix after a spin-exchange collision can be written in terms of the corresponding density matrix before the collision through a spin dependent scattering matrix, S;

$$\rho'(e,A) = S\, \rho(e,A)\, S^{\dagger},$$

where $\rho(e,A)$ is the outer product of $\rho(e)$ and $\rho(A)$.[46] Explicitly the matrix elements of S are written

$$\langle \vec{k}'s' | S | \vec{k}s \rangle = \langle \vec{k}'s' | \vec{k}s \rangle + 2\pi i \left(\frac{2\pi \hbar^2}{mL^3} \right) \delta(E - E') \langle \vec{k}'s' | M | \vec{k}s \rangle ,^{47}$$

where $\hbar\vec{k}$ and $\hbar\vec{k}'$ are the initial and final momenta of the electron with respect to the alkali atom. Box normalization is assumed and M is the reduced mass. The operator $\mathcal{M}$ is explicitly written in terms of both the singlet and triplet scattering amplitudes, $f_1(\Theta)$ and $f_3(\Theta)$ and the singlet and triplet projection operators P_1 and P_3,

$$\mathcal{M} = f_1(\Theta)\, P_1 + f_3(\Theta)\, P_3 .$$

Explicitly,

$$f_1(\Theta) = \frac{1}{2ik} \sum_{\ell=0}^{\infty} (2\ell+1)\left(e^{2i\delta_\ell^1} - 1\right) P_\ell(\cos\Theta),$$

$$f_3(\Theta) = \frac{1}{2ik} \sum_{\ell=0}^{\infty} (2\ell+1)\left(e^{2i\delta_\ell^3} - 1\right) P_\ell(\cos\Theta),$$

$$P_1 = \frac{1}{4}\left(1 - \vec{\sigma}_e \cdot \vec{\sigma}_A\right),$$

and

$$P_3 = \frac{1}{4}\left(3 + \vec{\sigma}_e \cdot \vec{\sigma}_A\right),$$

where δ_ℓ^1 and δ_ℓ^3 are the singlet and triplet scattering phase shifts.

From here the procedure consists of writing down $\rho(e,A)$, including momentum states, applying S, and obtaining the spin-state density matrix after a spin-exchange collision by tracing over the momentum index,

$$\langle s' | \rho'(e,A) | s \rangle = \sum_{\vec{k}} \langle \vec{k}\, s' | S\, \rho(e,A)\, S^\dagger | \vec{k}\, s \rangle .$$

After considerable algebra, this leads to an equation of motion for $\langle s' | \rho(e,A) | s \rangle$, then by tracing over the spin states of the electron, an equation of motion for $\rho(A)$ due to spin-exchange collisions with electrons is obtained, similarly, by tracing over the spin states of the alkali atom, the $\rho(e)$ equation of motion is obtained, i.e.

$$\frac{d\rho(A)}{dt} = \begin{pmatrix} \frac{P(e) - P(A)}{2T_{eA}} & 0 \\ 0 & \frac{P(A) - P(e)}{2T_{eA}} \end{pmatrix},$$

and

$$\frac{d\rho(e)}{dt} = \begin{pmatrix} \frac{P(A) - P(e)}{2T_{ee}} & -\frac{1 - iK P(A)}{T_{ee}} \rho_{12}(e) \\ -\frac{1 + iK P(A)}{T_{ee}} \rho_{21}(e) & \frac{P(e) - P(A)}{2T_{ee}} \end{pmatrix},$$

which lead immediately to the equations coupling the electron and alkali atom polarization through spin-exchange collisions,

$$\frac{dP(A)}{dt} = \frac{P(e) - P(A)}{T_{eA}},$$

and

$$\frac{dP(e)}{dt} = \frac{P(A) - P(e)}{T_{ee}}.$$

It is of interest to point out that the presence of the imaginary term in $\frac{d\rho(e)}{dt}$ gives rise to a frequency shift in the electron resonance. The term K was defined by B H P,

$$K \equiv \frac{\pi}{2\sigma_{SE}k^2} \sum_{l=0}^{\infty} (2l+1) \sin 2\left(\delta_l^3 - \delta_l^1\right),$$

where as shown in appendix I,

$$\sigma_{SE} = \frac{1}{4}\int |f_3(\theta) - f_1(\theta)|^2 d\Omega = \frac{\pi}{k^2}\sum_{l=0}^{\infty}(2l+1)\sin^2\left(\delta_l^3 - \delta_l^1\right).$$

The relaxation rates $\frac{1}{T_{eA}}$ and $\frac{1}{T_{ee}}$ are defined as follows:

$$\frac{1}{T_{eA}} = v_{eA} N_e \sigma_{SE},$$

and

$$\frac{1}{T_{ee}} = v_{eA} N_A \sigma_{SE},$$

where v_{eA} is the electron velocity, N_e is the number of electrons/cc in the sample, and N_A is the number of alkali atoms/cc in the cell.

All other relaxation mechanisms such as buffer gas disorientation collisions and wall collisions are phenomenologically introduced through the equations

$$\frac{d\rho(e)}{dt} = \begin{pmatrix} \frac{1}{2} - \rho_{11}(e) & -\rho_{12}(e) \\ \hline T_{1e} & T_{2e} \\ -\rho_{21}(e) & \frac{1}{2} - \rho_{22}(e) \\ \hline T_{2e} & T_{1e} \end{pmatrix},$$

and

$$\frac{d\rho(A)}{dt} = \begin{pmatrix} \frac{1}{2} - \rho_{11}(A) & -\rho_{12}(A) \\ \hline T_{1A} & T_{2A} \\ \rho_{21}(A) & \frac{1}{2} - \rho_{22}(A) \\ \hline T_{2A} & T_{1A} \end{pmatrix} .$$

Here T_{1e} and T_{1A} are the usual longitudinal relaxation times that appear in the Bloch Equations,[49] and T_{2e} and T_{2A} are the transverse relaxation times; again, e refers to the electrons, and A refers to the alkali atoms.

The effect of the transverse rf magnetic field is now discussed. The rf is applied at the resonance frequency of the electrons, depolarizing them. This depolarization is passed on to the alkali atoms by spin-exchange collisions. The first step then of incorporating the rf field into the model involves calculating the equation of motion of the electron density matrix, under the influence of the rf. The effect of the transverse rf magnetic field on the electron density matrix is most easily calculated by transforming to a reference frame that rotates with the rf field. The nice feature of this method is that in that rotating frame the time dependence of the magnetic fields is removed.

However, a linear oscillating rf was used in the present experiment. The rf field applied along the x axis can be expressed

$$\vec{H}_1 = 2 H_1 \hat{i} \cos \omega t .$$

This can be rewritten

$$\vec{H}_1 = H_1 \hat{i} \cos\omega t + H_1 \hat{j} \sin\omega t$$
$$+ H_1 \hat{i} \cos\omega t - H_1 \hat{j} \sin\omega t$$

which represents two fields rotating in opposite directions. The electrons, however, have a unique precession direction about the static field $\vec{H}_o$ determined by their magnetic moments. Thus, at resonance, one of the rotating components rotates in the same sense as the spins, and one rotates in the opposite sense. The counter rotating field is neglected to first order in H_1. This is justified only for $H_1 \ll H_o$, because the counter rotating term causes the resonant frequency to be shifted to a new value,

$$\omega = \omega_o \left[1 + \left(\frac{H_1}{2H_o} \right)^2 \right] .$$

This is known as the Bloch-Siegert Effect.[50] In the present experiment, the condition $H_1 \ll H_o$ was satisfied.

By using the transformation

$$\bar{\rho}(e) = e^{\frac{i\sigma_z \omega t}{2}} \rho(e) e^{-\frac{i\sigma_z \omega t}{2}},$$

B H P transform the lab frame equation,

$$i\hbar \dot{\rho}(e) = [\mathcal{H}_{LAB}, \rho(e)],$$

to the rotating frame. H_{lab} is the Hamiltonian for an electron in lab frame fields,

$$\mathcal{H}_{LAB} = + \frac{\hbar\omega_o}{2} + \sigma_x \hbar\omega_1 \cos\omega t,$$

where

$$\omega_o = - \frac{g_J \mu_o H_o}{\hbar} ,$$

and

$$\omega_1 = - \frac{g_J \mu_o H_1}{\hbar} ,$$

are the Larmor frequencies of the electrons in the fields of magnitude H_o and H_1, and μ_o is the Bohr Magneton.

Following this prescription, equations of motion for the electron density matrix elements in the rotating frame are found. The spin-exchange and other electron relaxation equations are then transformed to the rotating frame and added to this result. The final result of these manipulations, when solved at equilibrium, gives a relation between P(e) and P(A),

$$\frac{P(A)}{T_{ee}} = \left[\frac{1}{T_{1e}} + \frac{1}{T_{ee}} + \frac{\omega_1^2 \tau_2}{1 + \tau_2^2 (\omega_o - \delta\omega_o - \omega)^2} \right] P(e),$$

where

$$\frac{1}{\tau_2} = \frac{1}{T_{1e}} + \frac{1}{T_{ee}} ,$$

and

$$\delta\omega_o = 2\pi \delta\nu_o = \frac{P(A)}{T_{ee}} K .$$

Note that P(A) and P(e), the alkali and electron polarizations, are the same as viewed from both the lab or rotating frame if observations are made along the z axis, because the rotation operator used leaves P(A) and P(e) unchanged. Also note that $\delta\omega_o$ is a shift in the electron resonance frequency.

The pumping light contribution to the signal is now included. As is shown in appendix II the equation of motion for the z average alkali polarization, $\langle P(A) \rangle$, assuming complete reorientation in the excited state, under the influences of the pumping light is

$$\left(\frac{\langle d\, P(A) \rangle}{dt} \right)_{PUMP.} = \frac{1}{T_p} \left[1 - \langle P(A) \rangle \right],$$

where T_p is the pumping time. The spin-exchange and other alkali relaxation equations are averaged over z and are added to $\left\langle \frac{d\, P(A)}{dt} \right\rangle_{PUMP}$ to give an expression for the rate of change of $\langle P(A) \rangle$ due to pumping, spin-exchange collisions with electrons, and other disorienting collisions:

$$\left\langle \frac{d\, P(A)}{dt} \right\rangle_{TOT} = \left\langle \frac{\partial\, P(A)}{\partial t} \right\rangle_{PUMP} + \left\langle \frac{\partial\, P(A)}{\partial t} \right\rangle_{S.E.} + \left\langle \frac{\partial\, P(A)}{\partial t} \right\rangle_{\substack{OTHER \\ RELAX.}},$$

or

$$\left\langle \frac{d\, P(A)}{dt} \right\rangle_{TOT} = \frac{1}{T_p} - \frac{\langle P(A) \rangle}{T_p} + \frac{\langle P(e) \rangle - \langle P(A) \rangle}{T_{eA}} - \frac{\langle P(A) \rangle}{T_{1A}}.$$

Looking at the equilibrium situation for this equation,

$$\left\langle \frac{d\, P(A)}{dt} \right\rangle_{TOT} = 0,$$

and recalling and z averaging the rf equation gives two simultaneous equations which can be solved for $\langle P(A)\rangle$ and $\langle P(e)\rangle$:

$$0 = \frac{-\langle P(A)\rangle}{T_p} + \frac{1}{T_p} + \frac{\langle P(e)\rangle - \langle P(A)\rangle}{T_{eA}} - \frac{\langle P(A)\rangle}{T_{1A}} ,$$

and

$$\frac{\langle P(A)\rangle}{T_{ee}} = \left[\frac{1}{T_{1e}} + \frac{1}{T_{ee}} + \frac{\omega_1^2 T_2}{1 + T_2^2(\omega_0 - \delta\omega_0 - \omega)^2}\right]\langle P(e)\rangle .$$

If one now defines $\langle \delta P(A)\rangle$ as

$$\langle \delta P(A)\rangle = \langle P(A)\rangle_0 - \langle P(A)\rangle ,$$

where $\langle P(A)\rangle_0$ is the equilibrium alkali atom polarization in the absence of any rf, and $\langle P(A)\rangle$ is the corresponding equilibrium polarization when the rf is on, then, with a considerable amount of tedious algebra, a solution for $\langle \delta P(A)\rangle$ is obtained. Substituting the solution into

$$\delta I_T = \frac{A z_0 N_A}{T_p} \langle \delta P(A)\rangle ,$$

gives an expression for the predicted electron spin-exchange signal,

$$\delta I_T = -\frac{A z_0 N_A}{T_p^2} \frac{\frac{T_1}{T_{ee} T_{eA}}}{\left(\frac{1}{T_p} + \frac{1}{T_{eA}} + \frac{1}{T_{1A}}\right)^2} \frac{\omega_1^2 T_1 T_2}{1 + \omega_1^2 T_1 T_2 + (\omega_0 - \delta\omega_0 - \omega)^2 T_2^2} ,$$

where τ_1 is given by

$$\tau_1 = \frac{\frac{1}{\tau_P} + \frac{1}{\tau_{eA}} + \frac{1}{\tau_{iA}}}{\left(\frac{1}{\tau_{ie}} + \frac{1}{\tau_{ee}}\right)\left(\frac{1}{\tau_P} + \frac{1}{\tau_{iA}}\right) + \frac{1}{\tau_{ie}\,\tau_{eA}}} \quad .$$

This is an ideal juncture to briefly examine some results. δI_T represents a Lorentzian lineshape multiplied by a constant. The center of the Lorentzian has been shifted by an amount $\delta\omega_0$. These shifts indeed do exist and can be experimentally observed.[24,26] One also notices that the signal size varies directly as the number density of alkali atoms in the cell, the cell length, and the cross sectional area of the cell. It is also of interest to point out that the frequency shift

$$\delta\omega_0 = \frac{P(A)\,\pi}{\tau_{ee}\,\sigma_{SE}\,2k^2} \sum_{\ell=0}^{\infty} (2\ell+1)\,\sin 2\left(\delta_\ell^3 - \delta_\ell^1\right),$$

and the spin-exchange cross section

$$\sigma_{SE} = \frac{\pi}{k^2} \sum_{\ell=0}^{\infty} (2\ell+1)\,\sin^2\left(\delta_\ell^3 - \delta_\ell^1\right),$$

are both functions of the singlet and triplet scattering amplitudes, so that measurements of $\delta\omega_0$ and σ_{SE} can yield information concerning δ_ℓ^3 and δ_ℓ^1.

It should be pointed out that the δI_T result just expressed, differs slightly from that of B H P in that the constant term that multiplies the Lorentzian is different from theirs. The equation just written is what one obtains if the optical pumping cell is considered to be optically thin, which was the case throughout the course of this ex-

periment. B H P do not make this assumption but instead assume that the alkali atom polarization change, $\langle \delta P(A) \rangle$, produced by the rf set at the electron frequency is small.

From this theory, one sees that if the main electron spin-relaxation mechanism is spin-exchange, then the electron linewidth is given by

$$\Delta \nu = \frac{N_A \langle v_{eA} \sigma_{se} \rangle}{\pi} ,$$

where the brackets indicate a thermal average. Hence, if the alkali density is known, a measurement of the electron linewidth at a given temperature will determine $\langle v_{eA} \sigma_{se} \rangle$.

3. Nuclear Spin Effects

The spin-exchange theory of B H P just outlined was developed assuming a fictitious zero nuclear spin alkali atom. The validity of this approximation has been a point of discussion for several years. The following is a brief discussion of the effects of inclusion of nuclear spin.

The actual spin-exchange collision is indeed an interaction between the free electron and the valence electron of the alkali atom. Grossetete,[13] in a density matrix discussion of spin-exchange, shows that the polarization of the free electron immediately after a spin-exchange collision is a function of the electronic polarization of the alkali atom, and is independent of the nuclear spin, even though the electron spin and nuclear spin are coupled via the hyperfine interaction. The physical explanation of

this is that the spin-exchange collision time ($\sim 10^{-12}$ sec)[13] is much less than the hyperfine period of the alkali atom ($\frac{1}{A}$). Typical hyperfine periods are:[52, 53]

$$\frac{1}{A}\Big)_{Na} \approx \frac{1}{1.8 \times 10^9 Hz} = 5.6 \times 10^{-10} \text{ sec},$$

$$\frac{1}{A}\Big)_{Rb^{87}} \approx \frac{1}{6.8 \times 10^9 Hz} = 1.5 \times 10^{-10} \text{ sec},$$

and

$$\frac{1}{A}\Big)_{Rb^{85}} \approx \frac{1}{3.0 \times 10^9 Hz} = 3.3 \times 10^{-10} \text{ sec},$$

so that the condition holds. It appears, at first glance then, that there are no complications when nuclear spin effects are included. In this experiment, however, the electron resonance signal could not be observed directly, but only through changes in the alkali polarization induced by spin-exchange collisions between the depolarized electrons and the alkali atoms. It is necessary therefore to examine the evolution of the alkali atom polarization.

Grossetete,[13] Crampton,[54] and Gibbs[55,56] have all emphasized that nuclear spin does effect the alkali polarization. The connection between the electronic polarization and the nuclear spin is the hyperfine interaction. Crampton and Gibbs argue that between spin-exchange collisions, typically 10^{-4} sec, the valence electron and the nucleus "precess" around the total atomic angular momentum $\vec{F}$. Since the precession frequency or hyperfine frequency is $\sim 10^{10}$ Hz in most cases, the between-collision-time is relatively long.

During this hyperfine interaction, some of the electronic polarization may be transferred to the nucleus. This effectively changes the evolution of the electronic polarization from what it would be in the absence of nuclear spin. If this interaction is neglected, then as Lambert showed,[57] one indeed finds that the rate equation of P(A) includes no nuclear spin terms even for real alkali atoms which have nuclear spin.

In a detailed paper, Gibbs[55] pointed out that neglect of nuclear spin can lead to errors in the measurement of spin-exchange cross sections. He also argues that there are several ways that the alkali atoms can lose their polarization in between spin-exchange collisions. One of these is called electron randomization which can be brought about through disorienting collisions between buffer gas atoms and the alkali atoms. Gibbs states that if the main relaxation of the alkali polarization is through this process, then nuclear spin effects are negligible. One is not justified in assuming electron randomization was the dominant relaxation mechanism in the present experiment. However, no experimental evidence of a systematic error due to nuclear spin was detected. The tests performed are detailed in the measurement section of this thesis.

4. Linewidth Sources

Since this experiment involved the measurement of the width of a magnetic resonance line, it is important to

consider possible sources of the linewidth before interpreting physical information from the measurement. In general, a resonance line may be broadened by several mechanisms. Some of these are:

a. the natural lifetime of the state

b. Doppler broadening

c. magnetic field broadening

d. rf power broadening

e. collisional broadening

Each of the above possibilities will now be very briefly discussed in terms of its contribution to the electron linewidth in this experiment.

The natural lifetime of a polarized electron in a weak magnetic field ($\nu_e \sim 40\,kHz$) is extremely long ($\sim 10^{26}$ years).[58] The contribution of this to the linewidth is completely negligible.

One might expect that since the electrons and alkali atoms move at thermal velocities that a considerable Doppler broadening might be present. As shown by Dicke,[59] however, the presence of the buffer gas reduces the Doppler broadening to a very great extent. According to Dicke's result, the effect of non-disorienting buffer gas collisions is to reduce the Doppler broadening to a value of about $2.8\frac{L}{\lambda}$ times the normal Doppler width. L is the mean free path of the atoms and λ is the wavelength of the resonance photon. The conditions of this experiment were such that this collisional narrowing of the Doppler broadened line made the Doppler

broadening contribution negligible.

Magnetic field broadening was contributed by magnetic field inhomogeneities produced across the sample bulb by the Helmholtz coils. An estimate of the magnetic inhomogeneity was obtained by measuring the linewidth of the alkali Zeeman transitions in the limit of a very low rf. This linewidth was then multiplied by 2I + 1, ($\nu_{Zeeman} = \frac{\nu_{elect}}{(2I+1)}$). This gave an estimate of the maximum magnetic broadening. This was always $< 10\%$ of all electron linewidths. The actual inhomogeneous magnetic field contribution to the electron linewidth may indeed be less than the maximum estimate due to motional narrowing.[60]

The application of strong rf magnetic fields will in general broaden the resonance line because of saturation effects. Although the rf fields used in this experiment were quite weak, there was a substantial contribution to the electron linewidth due to rf power broadening. The strength of the rf field was experimentally determined each time a sample was run. The observed electron linewidth was then corrected to zero rf power by a method to be discussed later.

If spin-exchange collisions are the main broadening mechanism of the electron linewidth, then one expects

$$\Delta\nu = \frac{N_A}{\pi} N_{eA} \sigma_{SE} .$$

Earlier work showed that under experimental conditions similar to the ones in this experiment, the electron relaxation was dominated by spin-exchange collisions.[24] Similar

investigations were also undertaken in the present experiment. Checks performed on several samples showed that the electron linewidth was proportional to the alkali density over the range of linewidths measured.

If disorienting buffer gas collisions were the main source of electron relaxation, then one would expect that the electron linewidth would be a function of the buffer gas density. A variety of buffer gas types and pressures failed to produce any observable changes in the electron linewidth at room temperature.

On the basis of the above, it was concluded that the primary electron relaxation mechanism was spin-exchange collisions.

CHAPTER III

APPARATUS

The first part of this chapter will be concerned with a physical description of the apparatus. Following this a discussion of the signal detection method will be presented. The apparatus can be divided into several sections; the light source, the oven, and the signal detection electronics. We first discuss the Rb light source.

1. Light Sources

The Rb pumping light was provided by an rf driven Rb light bulb. The bulbs were made from 25 ml Pyrex flasks to each of which a one-inch long 6 mm o.d. stem was attached. The stem was used as a reservoir for the rubidium metal. The bulbs also contained a small amount (2-3 Torr) of research grade argon.[61] The stem of the bulb was placed in a Pyrex tube wrapped with 10 turns of heater wire. By varying the current in this wire, the Rb density in the bulb could be changed thus modifying the output characteristics of the lamp. The Pyrex heating tube was cemented in firebrick, and the brick was positioned so that the spherical section of the light bulb was centered inside a 7 turn coil of 3/16" o.d. copper tubing (figure 3). The coil dimensions were 4" length, and 2 1/2" diameter. The coil was actually

FIGURE 3

Rb LIGHT BULB

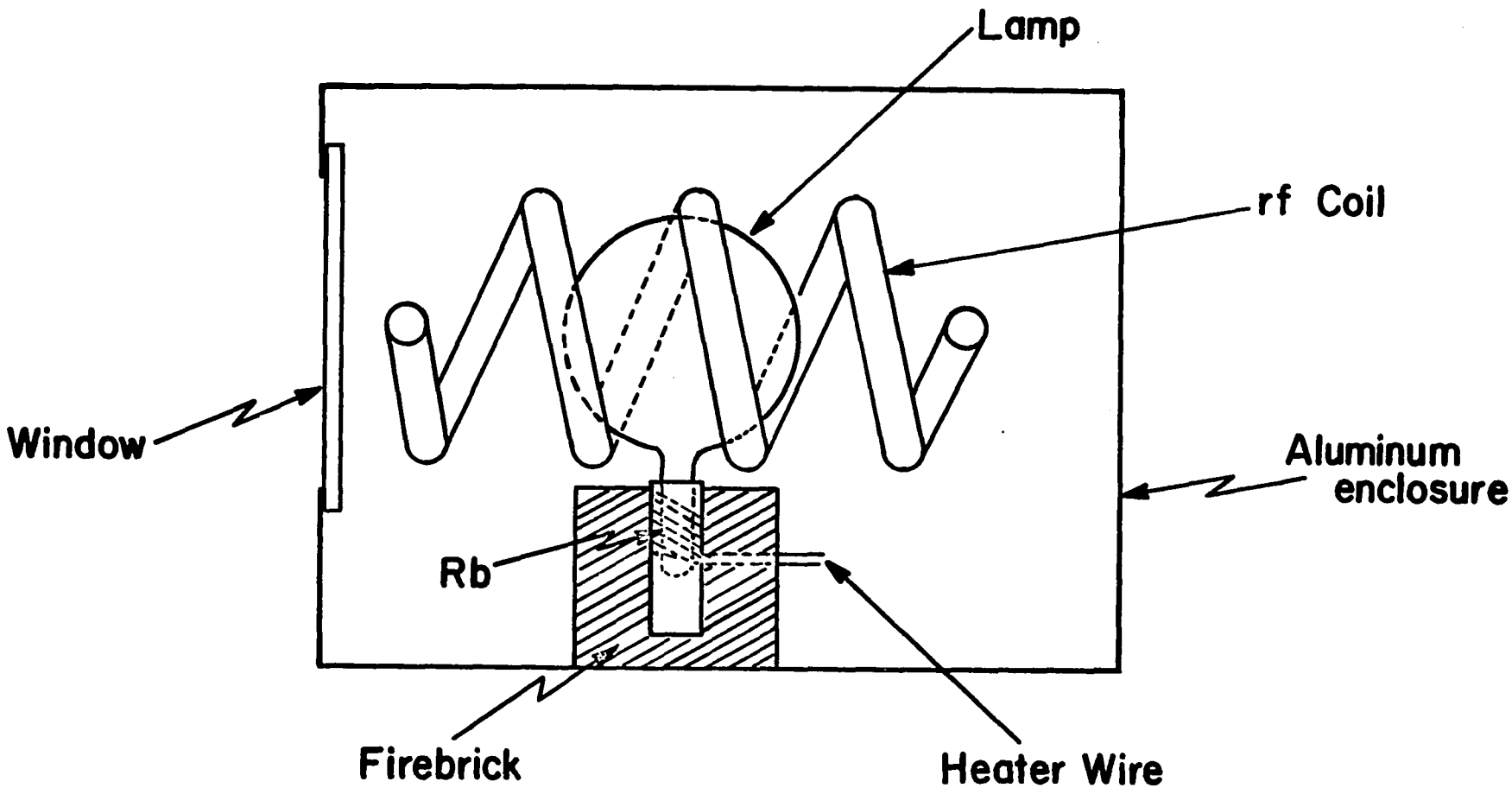
Lamp
rf Coil
Window
Aluminum
enclosure
Rb
Firebrick
Heater Wire

the inductor of a parallel L-C tank which was driven by a 10 MHz 50 Watt crystal controlled oscillator and amplifier. The rubidium bulb thus acted as a load for the amplifier.

In the operation of these lamps it is very important that the rubidium metal be kept entirely in the sidearm and out of the spherical region of the bulb. The lights operated in this manner are very quiet and noise spikes are minimal.

During the operation of the rubidium bulbs, the Rb vapor reacts with the Pyrex and turns it a deep brown color. This seems to have little effect upon the infrared ($7948\ \mathring{A}$)[34] pumping light intensity emitted, so that the sources are usually good even after they are quite opaque to visible light.

The Rb lamp was placed so that the light bulb was as close as possible to the focus of a 4" diameter convex lens. This produced an essentially parallel light beam. The lens holder also contained, in the order at which the pumping light intersected them, a Rb D_1 ($7948\mathring{A}$) interference filter, a linear polarizer, and a quarter wave plate. The D_1 filter attenuated the D_2 line and passed D_1 pumping light. The linear polaroid and quarter wave plate arrangement produce circularly polarized light when the fast optic axis of the 1/4 wave plate is at 45° with respect to the polarization plane of the polaroid.[62] The quarter wave plate was arranged so that it could be rotated

to give left circularly, right circularly, or linearly polarized light.

It was initially felt that sodium bulbs could be made and used in the same way. Sodium, however, reacts very strongly with Pyrex at 200° C or greater.[41] The walls quickly turn dark, and sometimes the reaction even cracks the Pyrex. In the process of constructing the light bulb, Na metal must be distilled into the bulb and then moved into the small sidearm. During the process of distilling the sodium, the bulb would "brown". Although the browning was not a serious problem for the rubidium, it was unacceptable for the sodium lamps. This was due to the fact that the sodium pumping light, 5896Å, lies in the visable part of the spectrum, hence the opaqueness would severely attenuate the pumping radiation intensity. Bulbs made of special alkali - resistant #1720 glass were tried without success. A method of coating the inside of the bulbs with Borax as discussed by Dushman[63] also failed.

The rf light source idea was abandoned, and the light source eventually used was a dc discharge lamp. The bulbs used were commercial G.E. Na-1 sodium light bulbs. Since the Na D_1 and D_2 lines lie very close together it is very difficult to filter out the D_2 line.[64] However, the pumping cycle becomes much more efficient if only D_1 light is used. The ratio of $\frac{D_1 \text{ intensity}}{D_2 \text{ intensity}}$ can be increased through the process of self reversal.[65] The usual case for self reversal in a lamp occurs because the

vapor in the central part of the lamp where the discharge occurs is hotter than the cooler outer regions. If there is sufficient vapor in these outer regions then it will absorb some of the resonance light coming from the central part of the bulb. The net effect is a decrease in the central part of the particular resonance line absorbed. This is very similar to the Fraunhofer dark lines that can be observed in a beam of sunlight.

To control the amount of self reversal, an oven was constructed which enclosed the light bulb. The oven consisted of a 6" diameter, 10" high, 1/8" thick brass tube (figure 4). A Pyrex window was provided in the side of the tube to allow the light to pass. An aluminum cover on the top of the tube contained a 10Ω conical heater on its underside. This provided the lamp-oven heat. The aluminum floor of the oven contained a hole through which the radiating section of the lamp protruded. The base section of the light bulb was placed in a socket below and outside the oven. The entire oven was lined with Fiberfrax.[66] A small concave mirror was placed behind the light bulb to enhance the output. The lamp was powered by a current regulated supply run at about 3.7 amps.

The lamp intensity was adjusted by varying the conical heater current until an optical pumping signal was found. The signal was maximized and the heater voltage was recorded. The lamp was run near or at this voltage for the entire experiment.

FIGURE 4

Na LIGHT SOURCE

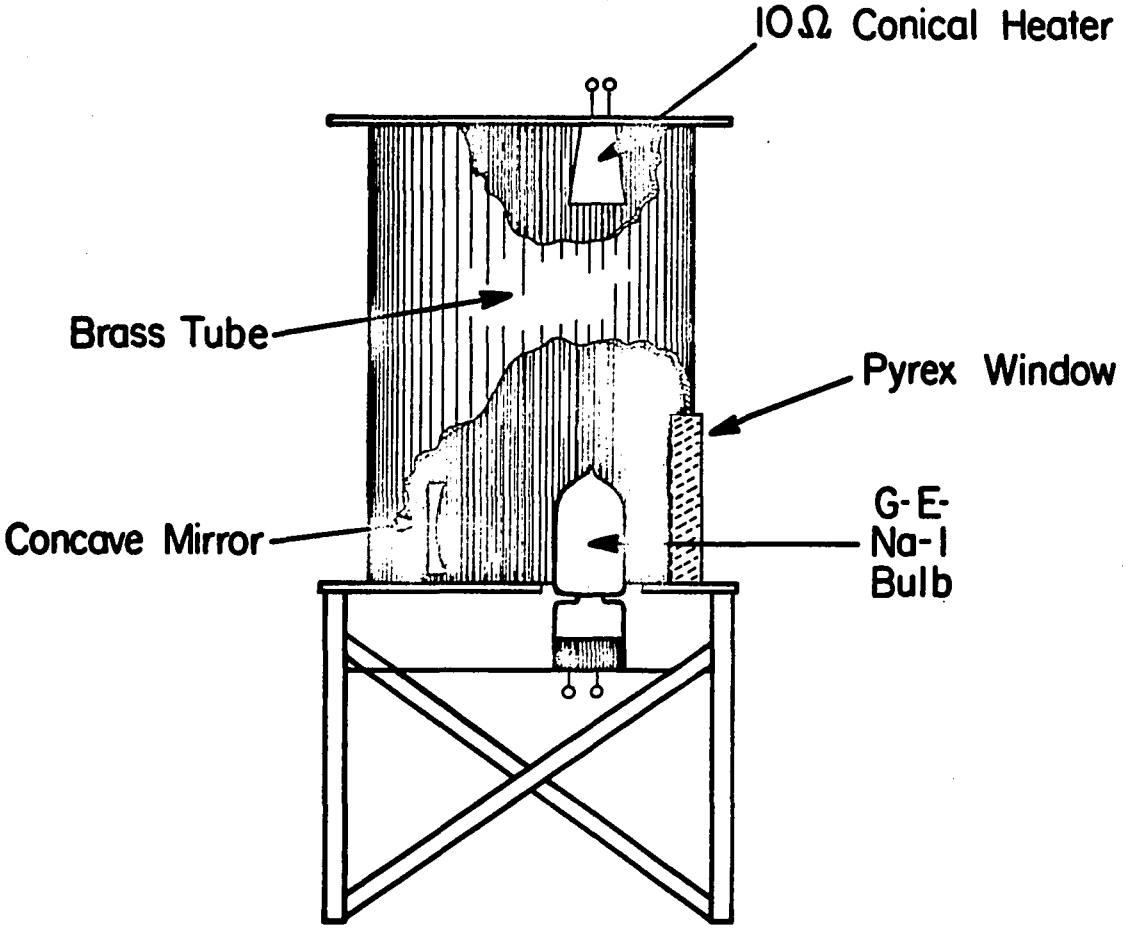
10Ω Conical Heater
Brass Tube
Pyrex Window
Concave Mirror
G-E-
Na-I
Bulb

The lamp was placed at the focus of the convex lens in a manner identical to the Rb lamp. The lens holder apparatus contained a linear polaroid and a Na 1/4 wave plate but no interference filter.

2. Shields and Oven

The actual region in which the optical pumping cell was positioned was surrounded by two concentric moly-permalloy cylinders in a manner introduced by Hanson and Pipkin in 1965.[67] The diameters of the cylinders were respectively 18 1/2" and 16 1/2". The lengths of the inner and outer shields were 40 1/8" and 42 1/8" long respectively. The inner shield was equipped with removable end caps, each cap having a 4" hole on center to permit passage of the pumping light. These cylinders shielded the pumping region from the Earth's field and from stray fields in the laboratory.

One inch holes were drilled along the diameter of the shields perpendicular to the axis at a point half way down the axis. These holes allowed a white light beam to traverse the pumping cell perpendicular to the pumping beam, (figure 5).

An 8-turn circular pair of Helmholtz coils was wound from #18 Teflon insulated wire against the inside walls of the inner shield to provide an axial magnetic field.

Inside the Helmholtz pair an oven was constructed.

FIGURE 5

BLOCK DIAGRAM OF APPARATUS

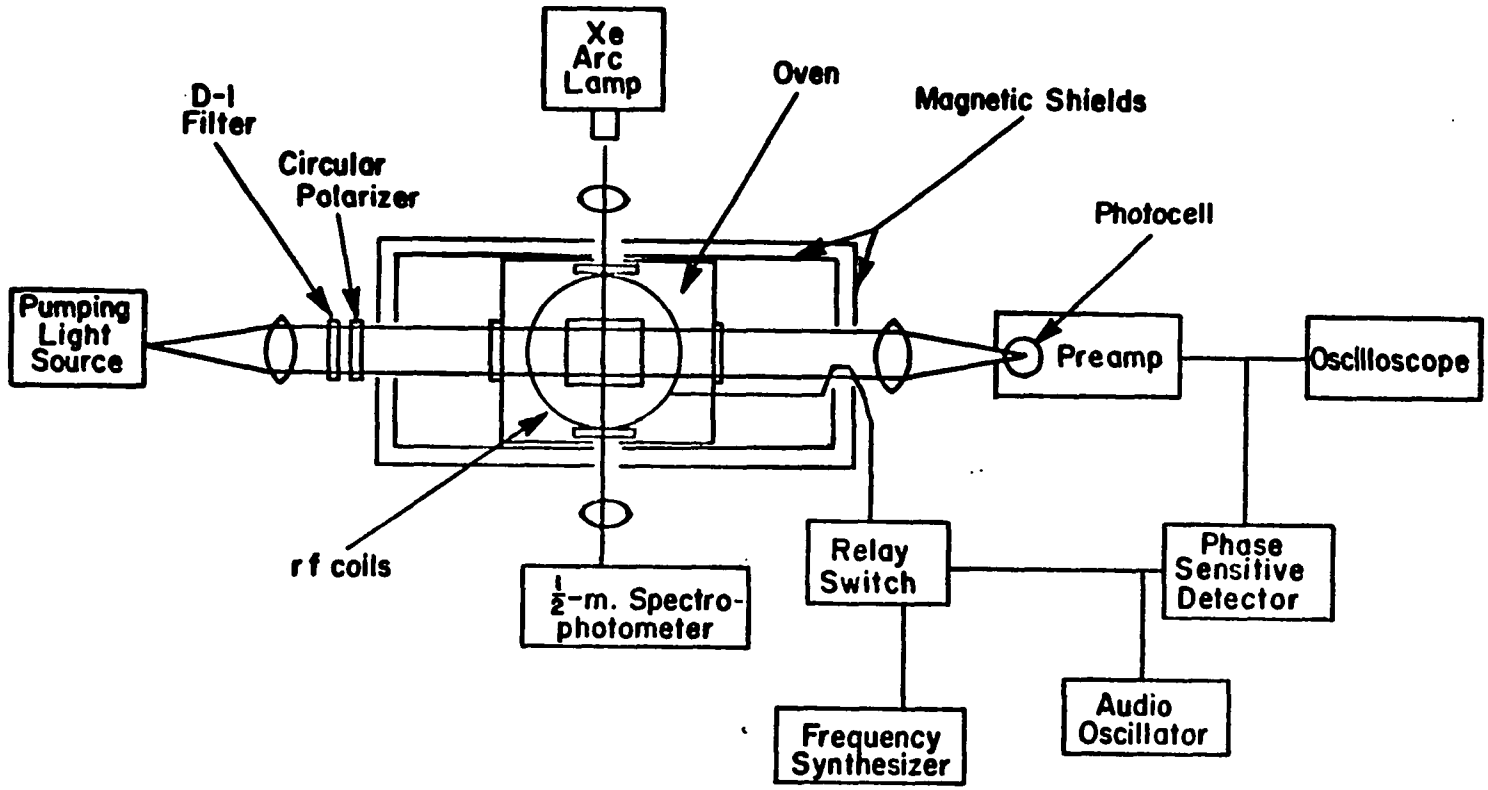
Xe Arc Lamp
Oven
Magnetic Shields
D-I Filter
Circular Polarizer
Photocell
Pumping Light Source
Preamp
Oscilloscope
r f coils
½-m. Spectro-photometer
Relay Switch
Phase Sensitive Detector
Frequency Synthesizer
Audio Oscillator

Since temperatures of several hundred degrees centigrade were desired, oven was built from non-magnetic firebrick.[68] The oven contained four, three-inch diameter Pyrex windows. Two windows were along the pumping axis to allow the pumping light to pass. (One of these, the front window, was in a firebrick door which could be removed to change samples.) The other two windows were on the side of the oven perpendicular to the pumping beam, but in line with the small holes in the sides of the shields. These two windows let the sampling white light beam pass. The oven also contained a Pyrex lens cemented into the firebrick wall which converged the white light beam after it had traversed the sample.

Three carbon-silicon heating rods near the oven ceiling and a horseshoe-shaped heating coil on the oven floor provided the heat for the elevated temperature work. The ceiling and floor heaters were independently controlled to reduce temperature gradients.

The oven also contained an 8" diameter one-turn Helmholtz pair to produce an rf field perpendicular to the pumping axis. These rf coils were made from chromel "A" heater wire to prevent damage at high temperatures.

The floor firebricks contained a Pyrex cooling tube which ran outside the oven to an external, pressurized air supply (figure 6). The tube contained a small pocket into which fitted the sidearm of the samples as previously described. Cool air could be blown through the tube to

FIGURE 6

COOLING TUBE CONFIGURATION

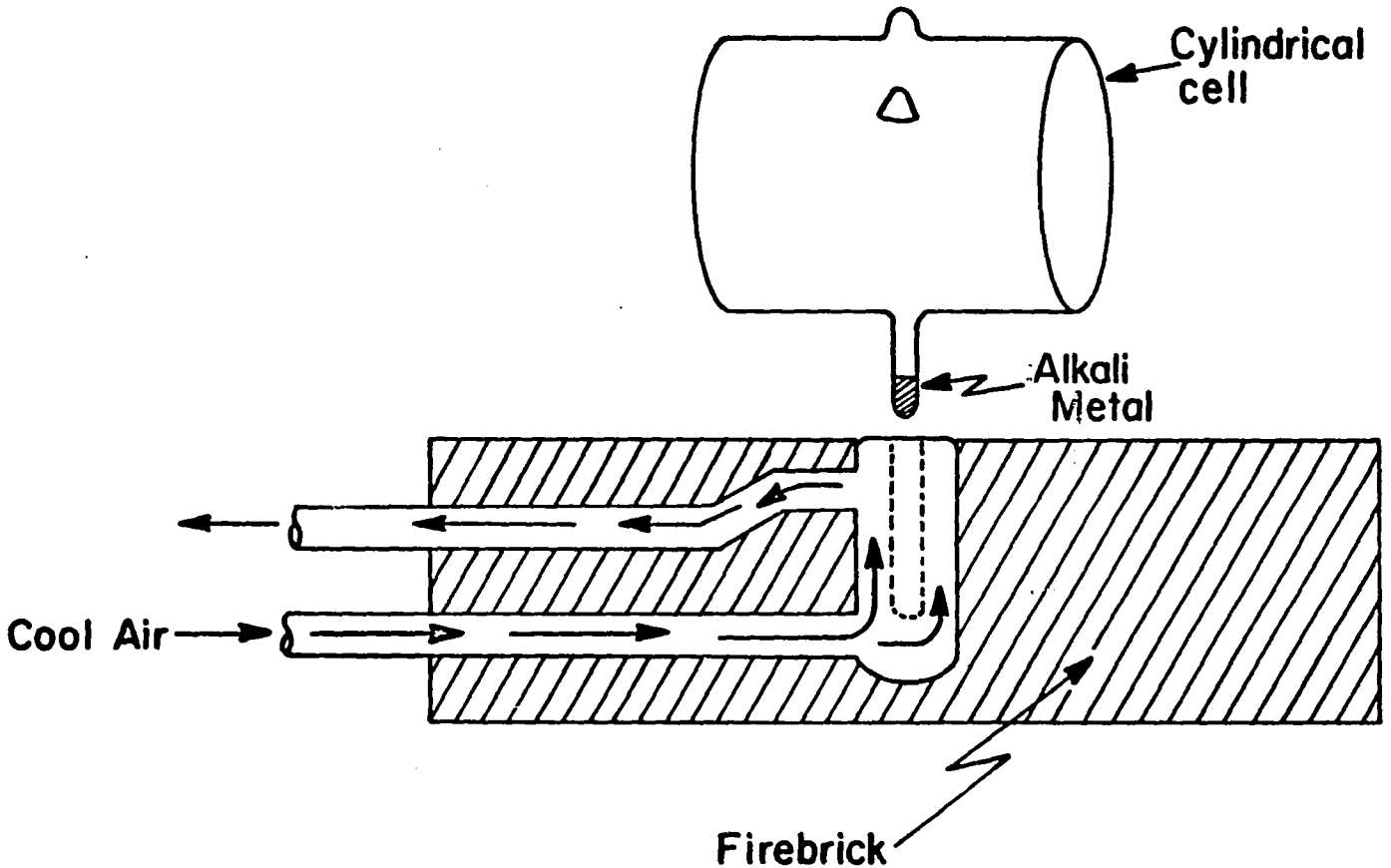
Cylindrical cell
Alkali Metal
Cool Air
Firebrick

cool the alkali reservoir sidearm of the pumping cell. This allowed the alkali reservoir temperature, hence the alkali density in the cell, to be controlled independently from the oven temperature. This is the principle of the high temperature optical pumping technique mentioned earlier.

Three platinum-platinum, 10% rhodium thermocouples were placed in the oven, one each, touching the bottom, middle, and top of the cell. The reference temperature was a distilled water ice bath. The thermocouples were checked against each other in ice water and in boiling water with better than $1^{o}C$ agreement. The emf produced by the thermocouples was read on a Leeds and Northrup potentiometer-galvanometer in conjunction with a Weston Model 4 standard cell. For convenience the potentiometer was set at the emf of a particular desired temperature. The output of the potentiometer (the difference between the set emf and the emf being generated by the thermocouple) was connected to a Kiethley 151R Null Detector. The null detector has a dc output which was fed into a flip-flop circuit.[69] The null detector output would swing positive or negative depending upon the emf generated by the thermocouple, i.e. the temperature in the oven. This positive and negative swing would activate the flip-flop circuit which was connected to a relay that was in series with the power lines to the oven heaters. The flip-flop was adjusted to function at the desired temperature $\pm$ 25° C,

i.e. as the temperature rose to 25° C above the temperature initially set on the potentiometer the oven heaters would shut off and similarly they would come on again at 25° C below the set temperature.

3. Electron Signal Detection

The detection of the electron signal was accomplished by observing changes in the transmitted pumping light caused by the rf applied at the electron resonance frequency, ν elect.

$$\nu_{elect} = -\frac{g_s \mu_o H_o}{2\pi\hbar} .$$

The resonant rf causes the electrons to become depolarized, and through spin exchange collisions the alkali atoms lose their polarization. The depolarized alkali atoms absorb pumping light through the process of optical pumping which results in a decrease in the transmitted light. This then is the principle of the detection scheme, used by Dehmelt.[1]

The actual detection technique is described below. The rf, produced by a General Radio 1164A Frequency Synthesizer, was fed into both a Hewlett-Packard 5245L Counter and into a mercury relay. The relay was driven by a square wave which was derived from an amplifier clipping circuit that received a 10 Hz sine wave input from a Hewlett-Packard 200 CDR Signal Generator. The output of the H-P was also used as the external reference

for an EMC Model RJB Lock-in Amplifier. The output of the mercury relay (chopped rf) was connected in series to a pair of Hewlett-Packard rf attenuators (one 355D and one 355C) which allowed attenuation of the rf from 0-132 Db in integral steps. The GR has the nice feature of generating a constant output, independent of the attenuation. This means that the input of the attenuators was always constant. The output of the attenuators was directly coupled to the rf Helmholtz pair in the oven.

The transmitted pumping light was focused onto a phototube, (#929 for Na, and #6953 for Rb). The phototube circuit is shown in figure 7. The photocurrent was displayed on an RCA WV-84 microammeter in series with the phototube. The potential drop produced by the photocurrent across the 1 meg resistor was passed through a .01 microfarad capacitor to a Tektronix 122A Preamplifier. The preamplifier output was transmitted simultaneously into an oscilloscope and the lock-in amplifier.

The chopping of the resonant rf means that the transmitted light intensity has a 10 Hz variation, (the bulb absorbs some pumping light while the rf is on and becomes more transparent in the absence of rf). This signal is displayed directly on the scope. The lock-in amplifier rejects inputs not in phase with the 10 Hz signal. This greatly increases the signal-to-noise ratio. The a c signal is displayed on the lock-in meter as a d c voltage. A block diagram of the electronics is shown in

FIGURE 7

PHOTOTUBE CIRCUIT

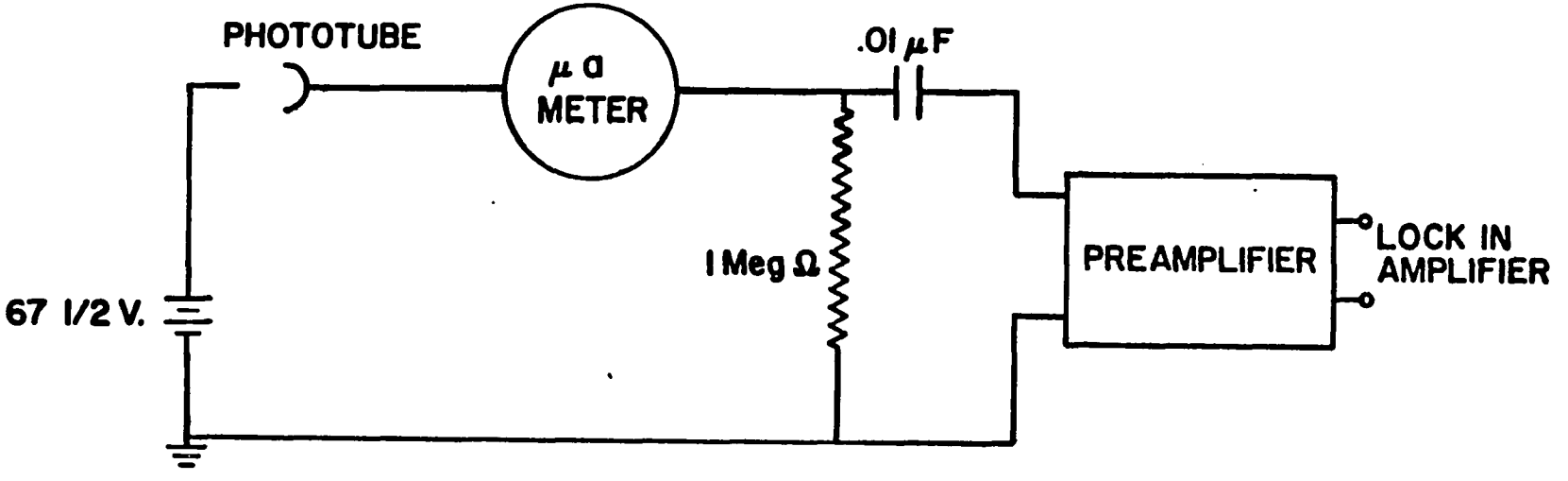
PHOTOTUBE
μa
METER
.01 μF
1 Meg Ω
67 1/2 V.
PREAMPLIFIER
LOCK IN
AMPLIFIER

figure 5.

4. Detection of the White Light Beam

The white light, produced by an Oriel C-60-50, 1-kW, Xe arc lamp, was passed through the sample perpendicular to the shields. The light beam was stopped down to one cm diameter just before it entered the optical pumping cell. The beam intersected the sample approximately half way up the sample. Great care was taken to place the bulbs in the oven so that they would be positioned the same for each run. After exiting the optical pumping cell, the beam passed through a Pyrex lens in the oven, the oven window, and was focused with a converging lens onto the slits of a 1/2 meter Jarrell-Ash 82-000 Ebert Scanning Spectrometer. The slit openings were set at 40 microns (40×10^{-6} meters). The output of the Jarrell-Ash was collected on the dynodes of a 7102 RCA photomultiplier tube whose photocurrent was displayed on a Kiethley 610-A Electrometer.

The fractional absorption of the white light by the D_1 or D_2 line of the particular alkali vapor in the cell was monitored on the electrometer. The spectrometer could be swept through the absorption lines, and if sufficient alkali vapor was in the cell, a decrease in the photomultiplier output was noted as the optical resonance lines were passed. The D_2 (7800Å) Rb line and the D_1 (5896Å) Na lines were monitored.

The fractional absorption of the white light was computed as follows. The following quantities were defined.

I_D ≡ dark current of the photomultiplier.

I_{max} ≡ photocurrent at zero absorption (off the resonance line).

I_{min} ≡ photocurrent at the center of the resonance line.

The fractional absorption is thus:

$$\frac{(I_{MAX} - I_D) - (I_{MIN} - I_D)}{(I_{MAX} - I_D)} \equiv \frac{\Delta I}{I}$$

The advantage of using the white light as a density monitor is that the fractional absorption is independent of temperature and pressure changes of the alkali absorption D lines. In general the presence of the buffer gas in the optical pumping cell will broaden and shift the center frequency of the absorption lines.[70] These effects increase linearly with pressure to first order. As a rule, one atmosphere of a foreign gas will broaden the strongest absorption lines to about 0.01 - 0.1 Å.[71] The pressures (10-60 Torr) used in this experiment reduce this value by more than an order of magnitude. Recent measurements[72] of the effects of He and Ne on the D_1 line of sodium give results that substantiate this rough calculation.

The shift and linebroadening were found to be about the same order of magnitude.[72]

Since the maximum resolution of the JA Spectrometer was 0.4Å, the recorded fractional absorption of the white light would be expected to be insensitive to any lineshape changes caused by the buffer gas. As a check, runs (described in the next chapter) were made on Rb cells with the slits open to 120 microns instead of the usual 40. This reduced the resolution of the spectrometer. Although this procedure reduced all the fractional absorptions measured, the ratio $\frac{\left(\frac{\Delta\nu_{elect}}{Fract.\,Ab.}\right)_{HIGH\ TEMP}}{\left(\frac{\Delta\nu_{elect}}{Fract.\,Ab}\right)_{ROOM\ TEMP}}$ (which is the quantity of interest in this experiment) was the same whether the two runs were made with the slits at 120 microns or at 40 microns. Also, the fractional absorption, at a given electron linewidth, at room temperature, was independent of buffer gas type (He, Ne) and pressure over the range 14-200 Torr. One must conclude that the fractional absorption always included the entire width of the alkali resonance line monitored.

CHAPTER IV

SAMPLE PREPARATION

The optical pumping cells used in this experiment were all prepared on a vacuum gas handling system. The cells were of two forms; some were 300 ml Pyrex flasks and the others were Pyrex cylinders. All the cells but one had a one inch long 6 mm o.d. stem on the bottom to serve as a reservoir for the alkali metal. The one bulb that had no stem will be discussed later.

The Pyrex samples were attached to the system as follows. The cells each had three constriction-seal offs, one of which was attached to the vacuum system. To one of the other constrictions a sealed U-tube containing alkali metal was connected. A glass slug was placed in the third sidearm, and a small capsule containing 1/3 C^{73} of tritium gas sealed with a break seal was connected to this sidearm.

The system was then evacuated and flamed with a Bunsen burner. When pressures of $\sim 5 \times 10^{-6}$ Torr were reached, the alkali metal was distilled into the sample. Bulbs intended for high temperatures necessitated having the alkali metal driven with a Bunsen burner into the small sidearm attached to the bottom of the cell. Samples to be used at temperatures not requiring independent temperature control of the alkali metal reservoir were well coated with alkali metal.

The distillation of the rubidium presented no problem but the sodium proved more difficult. Molten sodium reacts rapidly with Pyrex which turns the cells a dark opaque brown color. Some cells even cracked during preparation due to the sodium attacking the Pyrex. As a result, several cells were destroyed during preparation. Even when substantial amounts of sodium had been distilled successfully into a sample it was impossible to drive it into the tip without darkening the bulb.

This resulted in a change of technique, i.e. identical pairs of sodium cells (same size and buffer gas pressure) were made simultaneously. One cell was coated with liberal amounts of sodium and the other had only a thin layer of sodium driven into the tip. The former bulb would be used at $\sim 140^{\circ}$ C and the latter was a high temperature bulb. This method worked fine, as small amounts of sodium could be driven into the tip successfully.

This technique was not necessary for the rubidium samples because enough Rb could be put in the tip so that when it was desired to run the bulb at room temperature the Rb could be dumped in ample amounts from the tip into the rest of the cell.

After the distillation had been completed the U-tube distillation sidearm was sealed off and removed from the sample. The cell was then filled with a desired pressure of buffer gas such as neon or helium.[61] The pressure was measured by observing on a mercury manometer the buffer

gas pressure that zeroed a capacitance manometer. The filling temperature was also recorded.

The cell was then sealed from the system and removed. Then by means of the glass slug, the breakseal was ruptured and H^3 was allowed to diffuse into the bulb for about ten minutes. This sidearm was then sealed and removed. This procedure prevented any tritium from escaping either into the vacuum system or the laboratory atmosphere. The procedure is outlined in figure 8.

FIGURE 8

SAMPLE PREPARATION

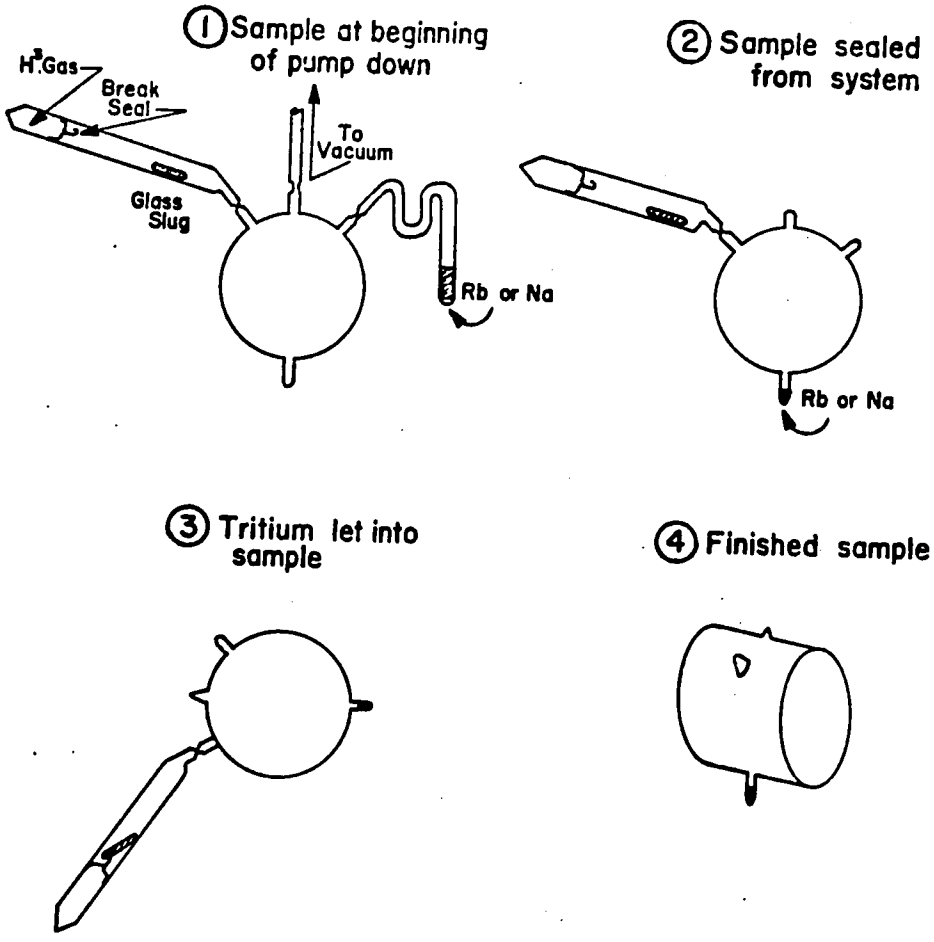
(1) Sample at beginning of pump down
H^3 Gas
Break Seal
Glass Slug
To Vacuum
Rb or Na
(2) Sample sealed from system
Rb or Na
(3) Tritium let into sample
(4) Finished sample

CHAPTER V

MEASUREMENTS AND DATA REDUCTION

1. Electron Linewidth and Fractional Absorption Measurements

The measurement techniques for both the Na and Rb experiments were identical. The cell was held at a fixed temperature and the electron linewidth was measured as a function of the fractional absorption of the white light beam.

The sample was heated to the desired temperature and the heaters were unplugged to keep sixty-cycle fields out of the optical pumping region. The alkali density was controlled by a stream of cool air as discussed earlier.

In the early phases of the experiment the data taking consisted of a temperature measurement, an electron linewidth measurement, followed by a white light fractional absorption measurement, followed by a linewidth, etc. This was repeated a few times as the temperature was monitored. The heaters were then turned on, and after heating, the process was repeated. The average temperature drop during this procedure was 25°C. A single datum point consisted of the average of a pair of linewidth measurements sandwiched around a fractional absorption measurement. Data were also taken and reduced by averaging two fractional absorptions

for every linewidth. The results of these two methods were identical.

The procedure of pairing, in order, two electron linewidth measurements around a single fractional absorption, or vice-versa, was undertaken because as the cell cooled with the heaters off, the fractional absorptions and linewidths recorded would steadily drop. The rate at which the sample cooled was minimized by heating the oven to 550°C and allowing the firebricks to become hot. While measuring a single electron linewidth, the peak amplitude was checked twice, once before the half-power points were determined and once immediately after measuring the half-power points. If there was a difference in these two peak amplitudes, the linewidth measurement was discarded because the alkali density was changing too fast. A run consisted of a collection of about twenty datum points.

The room temperature data (25°C for Rb, 140°C for Na) were easier to collect, mainly because of the stability of the temperature. Temperature gradients across the samples were $\sim 5°C$ at 140°C and $\sim 1°C$ at 25°C.

2. Density Gradients

Since the white light beam sampled only a small section of the optical pumping sample, to infer that the alkali atom density of the entire sample was equal to that measured by the white light beam assumes that the alkali atom density was uniform across the cell.

Initial tests for gradient effects were made with Rb samples of several buffer gas pressures. Runs measuring the electron linewidth as a function of fractional absorption of white light were made at 25°C. Electron linewidth versus fractional absorption of linearly polarized pumping light measurements were also made. Linearly polarized pumping light was used because the absorption of the cell is proportional to 1 minus the alkali polarization,

$$A \propto [1 - P(A)] .$$

Linearly polarized light induces zero polarization, thus removing the Rb polarization dependence. These runs were then compared to identical runs made at -5°C. The results demonstrated that the ratio of the fractional absorption at -5°C to the fractional absorption at +25°C, both at the same electron linewidth, decreased with increasing buffer gas pressure. Here the term fractional absorption refers to both the white light and the pumping light. The interpretation of this result was that at -5°C the buffer gas atoms were preventing the vapor from diffusing from their source to the cold walls. Thus a higher density of alkali atoms existed near the bottom of the cell and the white light beam would therefore sample a lower density than the average density of the sample. No effect was seen in a low pressure 14 Torr Neon sample. However, in a sample containing 57 Torr Ne, effects of $> 50\%$ were observed. (In a subsequent test it was shown that the electron signal amplitude was independent of the density gradients which seems to imply that the

electrons "see" an average alkali density.)

To obtain a quantitative estimate of the density gradients in the cells, a shutter was installed in the pumping beam so that the pumping light intersected it just before passing through the focusing lens in front of the phototube. This shutter could selectively pass different sections of the pumping beam, allowing the fractional absorption of the pumping light to be observed for various sections of the optical pumping cell. Once again, the pumping light was linearly polarized when these measurements were made.

The gradient measurements were typically performed as follows. The alkali atom density in the cell was adjusted until there was no detectable optical pumping signal. This was called the "zero density" point. The quarter wave-plate was then rotated 45°, thus linearly polarizing the pumping beam. The transmitted light intensity at the zero density point was measured for the top half, bottom half, and the whole of the sample. These intensities were labelled respectively

$$I_T^\circ,\ I_B^\circ,\ \text{and}\ I_W^\circ\ .$$

The density in the cell was then allowed to increase until a pumping signal could be seen with circularly polarized light. At this time, an electron linewidth was measured. The light polarization was then made linear and the transmitted intensities were recorded, as before, as

I_T, I_B, and I_W. The fractional absorptions in the top half, bottom half, and whole of the sample were then computed:

$$\frac{\Delta I_T}{I_T^o} \equiv \frac{I_T^o - I_T}{I_T^o} ,$$

$$\frac{\Delta I_B}{I_B^o} \equiv \frac{I_B^o - I_B}{I_B^o} ,$$

and

$$\frac{\Delta I_W}{I_W^o} \equiv \frac{I_W^o - I_W}{I_W^o} .$$

One would expect that if the alkali atom density were uniform, then the fractional absorptions would be equal for all sections of the sample. This was the case for the bulbs coated with alkali metal in which the vapor effuses from all the coated walls.

For high temperature work, however, the Rb or Na must be contained in a small sidearm as described earlier. At elevated temperatures it was found that serious density gradients existed across the sample, the density in the bottom of the cell being higher than the density in the top of the cell. This meant that the alkali vapor was more dense near the small reservoir. The narrow white light beam density measurements could then be in serious error.

However, when the cell temperature was increased to

a point where residual alkali atoms adsorbed on the cell walls diffused from the walls into the cell, the density gradients became suddenly very small.

The consequence of this was that measurements could be taken at only two temperatures. The one being at temperatures at which the cell walls were coated (~25°C for Rb, ~140°C for Na), and the other at high temperatures where the cell walls emitted residual alkali atoms (~380°C for Rb, and ~ 450°C for Na). Measurements were attempted at median temperatures but the density gradients were too severe.

The runs thus eventually consisted of the above density gradient monitoring in addition to the electron linewidth and white light measurements. Throughout the course of a run, the zero density points were checked to insure that a reliable fractional absorption of the pumping light could be made. As an additional check, a second photocell was positioned next to the resonance lamp to continuously sample a portion of the light. Any sudden changes in the lamp output could then be detected. As the experiment evolved, it became clear that the lamps were very stable, thus the pumping light transmission at zero density was essentially constant throughout the run.

A second method was also used to measure the density gradients. This consisted of measuring the relative sizes of the Rb or Na Zeeman signals in various parts of the sample. In the low density limit the pumping signal amplitude

is proportional to the alkali atom density,

$$\int I_T = \frac{N_A Z_0 A}{\tau} \langle \int P(A) \rangle .$$

It is important to recognize that the shutter intersected the pumping light beam after the beam had passed through the cell, thus it did nothing to disturb the processes going on in the cell. From the above equation one sees that the observed signal is proportional to the alkali atom density of the section of the sample observed. The measurements of the signal sizes in the top half, bottom half, and whole of the bulb were in good agreement with the pumping light absorption density gradient checks.

The error in monitoring the alkali density in the cells with the white light beam was estimated to be $< 5\%$ in all data eventually used.

3. Extrapolation to Zero rf Power

An examination of the predicted electron signal,[24]

$$\int I_T = (\text{CONSTANT}) \left[\frac{\omega_1^2 T_1 T_2}{1 + (\omega_1)^2 T_1 T_2 + \left(\frac{\Delta\omega}{2}\right)^2 T_2^2} \right],$$

reveals that at the half power point

$$\frac{1}{T_2^2} = \left(\frac{\Delta\omega}{2}\right)^2 - \omega_1^2 \frac{T_1}{T_2} , \qquad (1.)$$

where

$$\Delta\omega \equiv 2(\omega_0 - \delta\omega_0 - \omega),$$

and T_1 and T_2 were previously defined. The experiments of B H P[24] showed that under experimental conditions similar to ours, spin-exchange collisions were the dominant relaxation mechanism.

Hence,

$$\frac{1}{T_2} = \frac{1}{T_{ee}} + \frac{1}{T_{1e}} \approx \frac{1}{T_{ee}} .$$

Equation (1) can be written

$$\frac{1}{T_2^2} = \pi^2\Delta\nu^2 - 4\pi^2\nu_1^2\frac{T_1}{T_2},$$

where

$$2\pi\Delta\nu = \Delta\omega,$$

and

$$2\pi\nu_1 = \omega_1 .$$

So we arrive at an expression for the electron linewidth due to spin-exchange

$$\frac{1}{\pi T_2} = \frac{1}{\pi T_{ee}} = \sqrt{(\Delta\nu)^2 - 4\nu_1^2\frac{T_1}{T_2}}$$

In this expression $\Delta\nu$ is the "raw" electron linewidth measured at the FWHM and $4\nu_1^2\frac{T_1}{T_2}$ is a measure of the rf field strength. The reduction of the electron linewidth data thus consisted of extrapolating to zero rf power.

A plot at constant temperature of $\left(\frac{\Delta\omega}{2}\right)^2$ as a function of ω_1^2 yielded a straight line of slope $\frac{T_1}{T_2}$ and

an intercept of $\left(\frac{1}{T_2}\right)^2$, see figure 9.

By recalling that

$$T_1 = \frac{T_{eA}^{-1} + T_p^{-1} + T_{1A}^{-1}}{\left(T_p^{-1} + T_{1A}^{-1}\right)\left(T_{ee}^{-1} + T_{1e}^{-1}\right) + T_{1e}^{-1} T_{eA}^{-1}}$$

it follows that if $\frac{1}{T_{1e}}$ is neglected,

$$\frac{T_1}{T_2} \approx \left(1 + \frac{T_{eA}^{-1}}{T_{1A}^{-1} + T_p^{-1}}\right) .$$

Earlier measurements of e - Rb spin-exchange collisions yielded a result

$$\frac{T_1}{T_2} = 1.0 \pm 0.1 .$$

Some bulbs used in the present experiments containing tritium gave slopes as high as

$$\frac{T_1}{T_2} = 2.0.$$

From the expression for $\frac{T_1}{T_2}$ one notes that if $\frac{1}{T_{eA}}$ is increased, $\frac{T_1}{T_2}$ will increase. Since $\frac{1}{T_{eA}}$ is proportional to the number density of electrons, the large slopes are explained by the presence of larger amounts of tritium.

The sodium cells gave slopes very nearly equal to unity in good agreement with previous measurements.[26]

The rf field strength ω_1, was determined by holding the rf at the center of the electron resonance and increasing the static field until the alkali Zeeman signal was reached. The trace seen on the oscilloscope (figure 1) showed the damped precession of the alkali atoms about the rf field of

FIGURE 9

PLOT OF $\left(\frac{\Delta\omega}{2}\right)^2$ VERSUS $(\omega_1)^2$

FOR A CELL CONTAINING Rb, Ne, AND H^3.

SAMPLE AT 25°C. THE SLOPE OF THE LINE IS $\frac{T_1}{T_2}$

AND THE INTERCEPT IS $\frac{1}{T_2^2}$

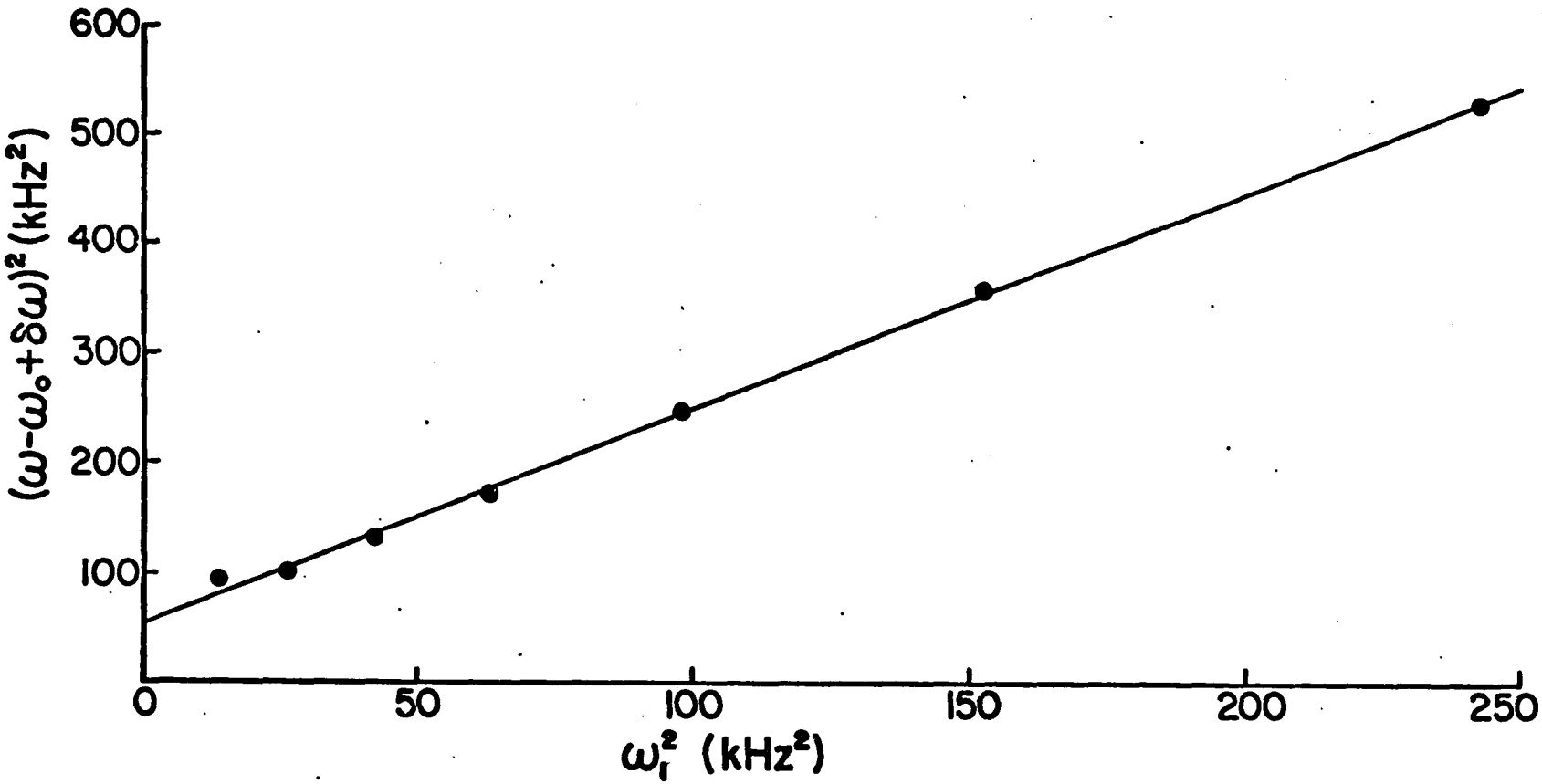
600
500
400
300
200
100
0
50
100
150
200
250
$(\omega-\omega_o+\delta\omega)^2$ (kHz^2)
ω_1^2 (kHz^2)

strength H_1. The precession frequency of the alkali atoms about H_1 was calculated by counting the wiggle frequency displayed on the scope. The electron angular frequency was then calculated from the relation,

$$\omega_1 = (2I+1)\, 2\pi \nu_1 \text{ (ALKALI)},$$

where I is the nuclear spin, and = 3/2 for Na and Rb.[87]

In most runs the electron linewidth was measured at a fixed rf strength so that the correction consisted of subtracting a constant amount $4\nu_1^2 \frac{T_1}{T_2}$ from each measured linewidth. Checks of $\frac{T_1}{T_2}$ at high temperature failed to produce any measurable effect, however, the rf field strength used was weak enough so that any changes that might have occurred were negligible.

4. Effect of Nuclear Spin

Two checks were performed in an attempt to detect a systematic effect due to nuclear spin. A pair of identical 300 ml spherical samples were prepared. Each contained 100 Torr He and 1/3 C of H^3. One cell contained isotopically pure Rb^{85} and the other contained pure Rb^{87}. These cells were run at room temperature and at fixed rf. The results of the electron linewidth versus fractional absorption of white light (figure 10) shows no measurable difference between the two plots.

A second test was performed with a sample that contained a large amount of H^3, 50 Torr of Neon, and Rb. A

FIGURE 10

PLOTS OF ELECTRON LINEWIDTHS

VS. FRACTIONAL ABSORPTIONS

FOR PURE Rb^{87} AND PURE Rb^{85}.

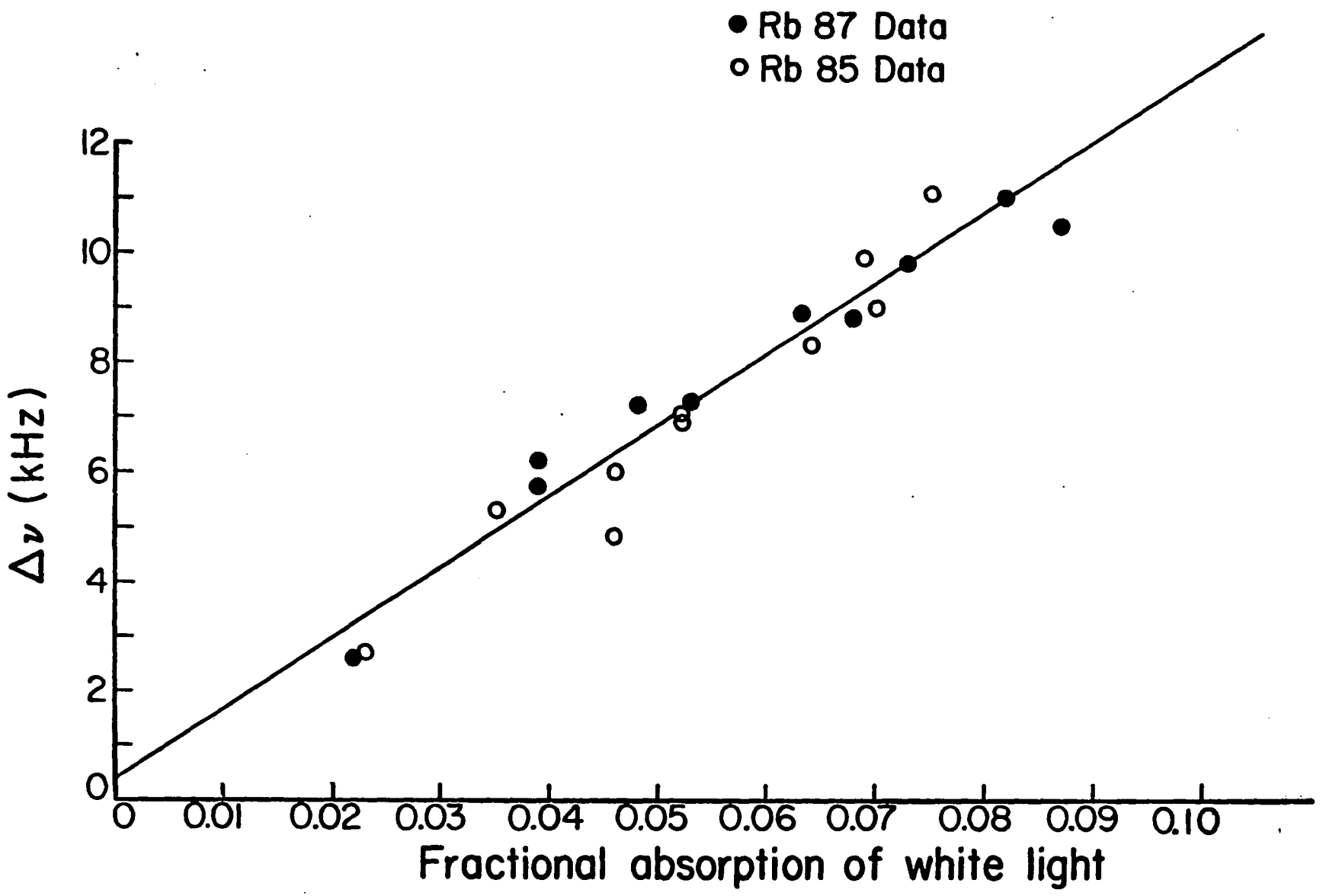
● Rb 87 Data
○ Rb 85 Data
Δν (kHz)
0
2
4
6
8
10
12
0
0.01
0.02
0.03
0.04
0.05
0.06
0.07
0.08
0.09
0.10
Fractional absorption of white light

run of $\left(\frac{\Delta\omega}{2}\right)^2$ vs ω_1^2 was made to determine T_1 and T_2, (figure 9). These values were then substituted into the δI_T expression for the linewidth which was derived for a nuclear spin = 0 alkali model. The predicted Lorentzian was then plotted. The predicted electron signal is shown as a solid curve in figure 11. The actual electron signal was then measured at a fixed rf power as a function of rf frequency ω . The observed electron line was then normalized at one point to the predicted curve. The result is shown in figure 11. The agreement between the measured and predicted signal is excellent.

On the basis of the above results, it seems unlikely that nuclear spin effects are noticeable within the experimental error of the experiment.

5. Frequency Shifts

The measurements of electron resonance frequency shifts due to spin-exchange collisions with Rb atoms were facilitated by noting that

$$\delta\nu_0 = \frac{P(A)\,K}{2\pi\,\tau_{ee}} ,$$

i.e. the sign of the frequency shift $\delta\nu_0$ changes when the sign of the alkali polarization is reversed. Since left and right circularly polarized pumping light produce alkali polarizations of opposite sign, the electron frequency shift can be observed by measuring the change in the frequency of the resonance peak due to a corresponding change in the alkali polarization.

FIGURE 11

PLOT OF THE LORENTZIAN LINESHAPE

CALCULATED FOR A PARTICULAR VALUE OF

ω_1 = 5.2 kHz FROM THE TIME CONSTANTS T_1 AND T_2

FROM FIGURE 9.

Amplitude (arbitrary units)
1
2
3
4
5
6
7
8
-10
-9
-8
-7
-6
-5
-4
-3
-2
-1
0
1
2
3
4
5
6
7
8
9
10
ν-ν₀ (kHz)

The frequency shift was measured at fixed Rb density and at various temperatures by measuring the center frequency of the resonance line, first with left then with right circularly polarized pumping light. One half the difference of these two center frequencies gave the value of the shift.[24]

The magnitude of the Rb polarization was estimated by measuring the absorption of the pumping light first by polarized Rb atoms, then by unpolarized Rb atoms. If one assumes that the absorption is proportional to $[1 - P(A)]$ then one can write

$$\frac{A_{bs}(\text{POL Rb})}{A_{bs}(\text{UNPOL Rb})} = \frac{[1 - P(R)]}{1} ,$$

so

$$P(R) = 1 - \frac{A_{bs}(\text{POL Rb})}{A_{bs}(\text{UNPOL Rb})} .$$

Since the static magnetic field was produced by a Helmholtz pair it was not possible (because of field inhomogenieties) to measure the relative amplitudes of the various Zeeman transitions to check the above estimate.

No frequency shift measurements were done for e-Na spin-exchange collisions because of the uncertainty in estimating the Na atom polarization.

6. Systematic Errors

A discussion of the possible systematic errors that were checked, follows. One of the worst sources initially

were the density gradients. They were reduced so that the estimated error was $< 5\%$.

The possibility that the white light beam might influence the electron linewidth was thoroughly investigated. No effect was observed.

One source of systematic error became apparent in the middle of the experiment. Until this time a lens outside the shields which focused the white light beam onto the slits of the spectrometer had been adjusted from time to time to obtain a maximum output from the photomultiplier at the beginning of a set of runs. The process of changing the lens position, however, varied the angle of incidence of the white light beam onto the slits. This changed the effective slit width as seen by the beam, hence causing variations in the fractional absorption. This was systematically checked by making high and "room" temperature runs with the lens held at one fixed position. The lens was then moved and the measurements were repeated. Although this shifted all the fractional absorptions, the ratio

$$\frac{\left(\frac{\Delta\nu}{\text{FRAC. AB.}}\right)_{\text{HIGH TEMP}}}{\left(\frac{\Delta\nu}{\text{FRAC. AB.}}\right)_{\text{ROOM TEMP}}}$$

remained constant. The conclusion was that if the lens or any part of the optical system were altered during any particular run then the measurements would not be reliable.

All previous data was discarded and new measurements were made on both Rb and Na.

The temperature measurements as stated earlier were obtained by measuring the temperature on the outside surface

of the sample. Dummy cells were constructed to determine what the temperature inside the sample was at a given outside temperature. One of the dummy cells of known volume contained a known pressure of gas and was connected to a manometer. The sample was heated while its outside temperature was monitored with thermocouples and the change in pressure was recorded on the manometer. The other dummy cell contained three thermocouples sealed inside the cell. These checks indicated that the error in temperature measurement at the highest temperatures was 25°C.

A possible source of error which should be mentioned is that the electrons may not actually be thermalized. However, previous experiments[24] and early phases of the present experiment[76] make this seem unlikely. B H P[24] showed that the electron linewidth at fixed Rb density was independent of buffer gas, buffer gas pressure, or whether the electrons were produced by an rf discharge or by H^3. In the present experiment both He and Ne were used and the pressures varied from 14 to 200 Torr. Some of these cells contained H^3 and others contained an rf discharge. Identical results were obtained at fixed Rb density in all cells within experimental error, i.e. electron linewidths were 1.3±0.2 kHz at 20 C.

CHAPTER VI

RESULTS

1. Linewidth vs. Fractional Absorption Results

The results of both the Rb and Na measurements are presented in this chapter. Typical sodium and rubidium data are presented in figures 12 and 13 respectively. In each of these figures the electron linewidth has been plotted at two temperatures (300° K and 660° K for Rb; 400° K and 725° K for Na) as a function of the white light fractional absorption. The zero alkali density intercept was taken to be the linewidth due to magnetic field inhomogeneity, (250Hz).

The results of the measured ratio of

$$\frac{\left(\frac{\Delta\nu}{N_A}\right)_{T^\circ K}}{\left(\frac{\Delta\nu}{N_A}\right)_{\text{ROOM TEMP.}}}$$

are presented in table 1. Here the term "room temperature" refers to the temperatures of the coated bulbs (300° K for Rb; 400° K for Na). Table 1 also contains the ratio of the mean electron velocities at the two temperatures measured. Table 1 represents an average of the data collected on different runs. The error assigned to

$$\frac{\left(\frac{\Delta\nu}{N_A}\right)_{T^\circ K}}{\left(\frac{\Delta\nu}{N_A}\right)_{\text{ROOM TEMP}}}$$

represents the spread in the total data collected. An examination of table 1 shows that within the experimental

FIGURE 12

PLOT OF THE ELECTRON LINEWIDTH

VERSUS THE FRACTIONAL ABSORPTION OF

WHITE LIGHT AT 400°K AND 725°K,

FOR e-Na COLLISIONS.

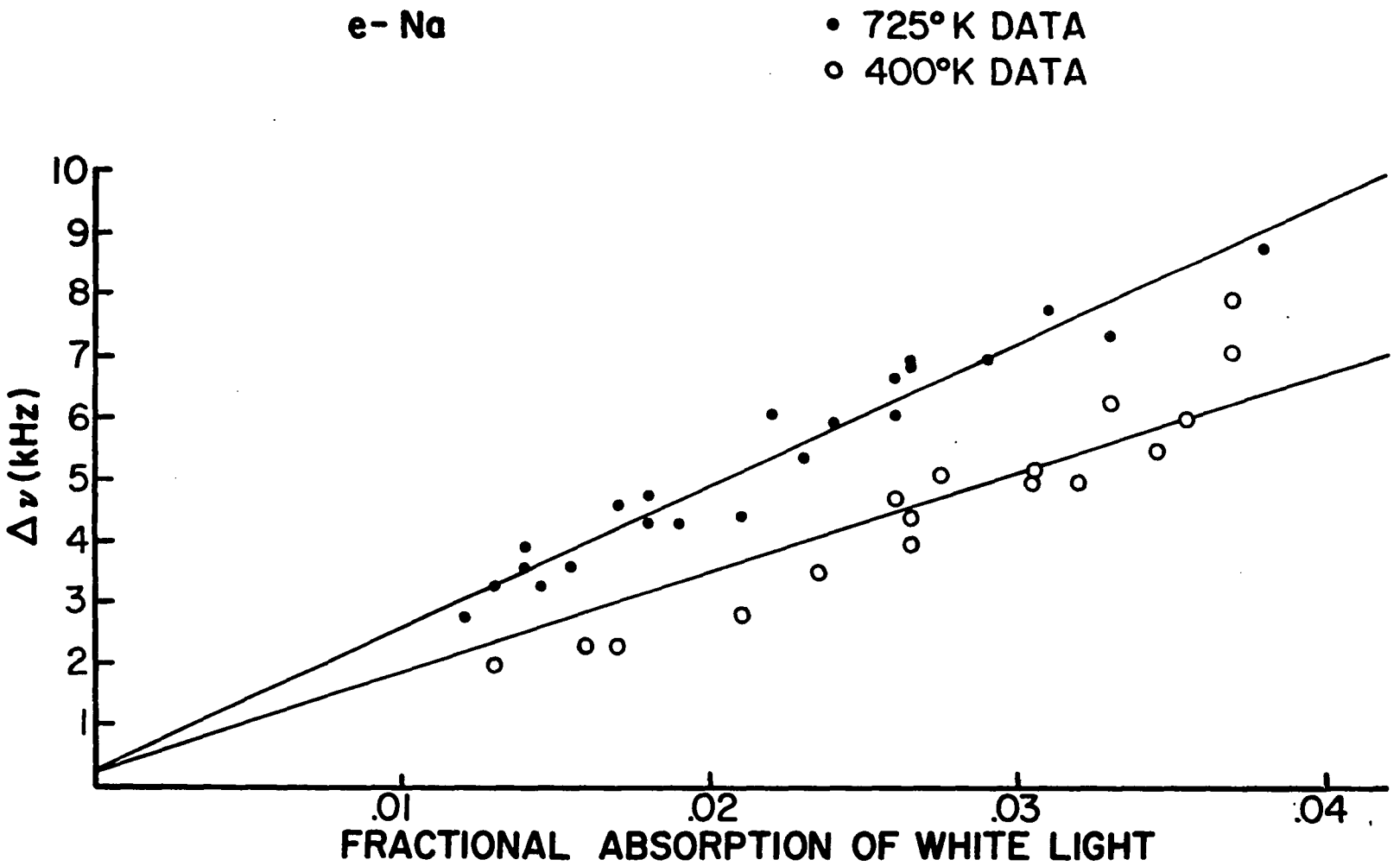
e- Na
• 725°K DATA
o 400°K DATA
10
9
8
7
6
5
4
3
2
1
Δν (kHz)
.01
.02
.03
.04
FRACTIONAL ABSORPTION OF WHITE LIGHT

FIGURE 13

PLOT OF THE ELECTRON LINEWIDTH

VERSUS THE FRACTIONAL ABSORPTION OF

WHITE LIGHT AT 300°K AND 660°K

FOR e-Rb COLLISIONS.

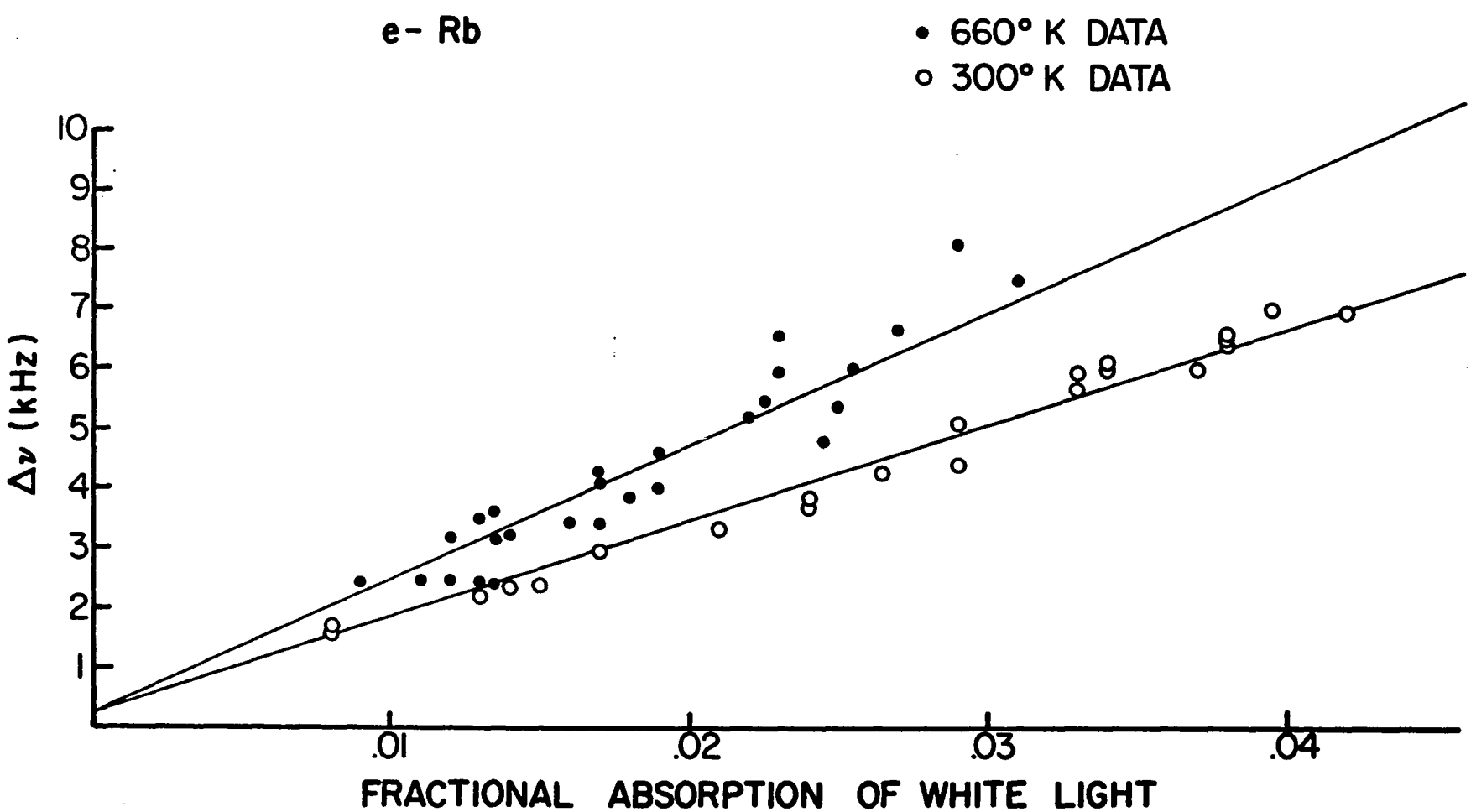
e- Rb
• 660° K DATA
o 300° K DATA
10
9
8
7
6
5
4
3
2
1
Δν (kHz)
.01
.02
.03
.04
FRACTIONAL ABSORPTION OF WHITE LIGHT

error, for both Na and Rb

$$\frac{\left(\frac{\Delta\nu}{N_A}\right)_{T^\circ K}}{\left(\frac{\Delta\nu}{N_A}\right)_{\substack{ROOM\\TEMP}}}$$

is proportional to the electron velocities over the temperature ranges measured. This means that the e-Rb, and e-Na spin-exchange cross sections are roughly constant over this range.

If one utilizes this information, then values at room temperature can be obtained for both the e-Rb and e-Na spin-exchange cross sections. In the expression

$$\frac{\Delta\nu}{N} = \langle v\, \sigma_{SE} \rangle \frac{1}{\pi}$$

the thermal average

$$\langle v\, \sigma_{SE} \rangle$$

can be reduced to

$$\langle v \rangle\, \sigma_{SE}$$

if the spin-exchange cross section is assumed constant. If the average or mean velocity is chosen, then

$$\langle v \rangle\, \sigma_{SE} = \sqrt{\frac{8}{\pi}\,\frac{kT}{m}}\;\sigma_{SE}$$

where k is Boltzmann's constant, T is the temperature in ^{o}K, and m is the electron mass. Hence

$$\sigma_{SE}\Big)_{\substack{ROOM\\TEMP}} = \frac{\Delta\nu}{N_A}\Big)_{\substack{ROOM\\TEMP}} \left(\frac{\pi m}{8kT}\right)^{\frac{1}{2}} (\pi)$$

The results of this calculation appear in table 2.

The results of the frequency shift measurements

are presented in table 3. Since the polarization estimates could not be rigorously checked, this data is intended to be only qualitative.

2. Comparison with Recent Theory

Recently, close-coupling calculations have been completed by Moores and Norcross[22, 23] for electron sodium collisions in the same energy range as measured in this paper. In table 4 their results are compared to the results of this experiment. The comparison of $\frac{\Delta\nu}{N}\Big)_{403^\circ K}$ shows that the observed linewidth is about a factor of three higher than predicted by Moores and Norcross. A source of error in the measurements of $\frac{\Delta\nu}{N}\Big)_{403^\circ K}$ is in the use of vapor pressure curves. It has been previously shown that the bare pyrex walls of a cell act as a sink for sodium vapor.[26] The vapor pressure however is defined as the pressure exerted at a given temperature on a saturated vapor by a vapor source. A saturated vapor is more difficult to produce if there is a constant sink for the vapor. Thus in order to obtain a number density for the sodium vapor by means of vapor pressure curves, one must reduce the uncoated area of the bulb as much as possible.

Mindful of this, a special cell was constructed to measure the sodium density at 400° K. This cell was approximately 75% coated with sodium metal and had no reservoir tip. Measurements of the electron linewidth

as a function of cell temperature followed the vapor pressure curve for sodium very well.

The measurements were made over very limited range of temperatures $\sim 15^{\circ}$ C. Over this narrow range, $\langle \sigma_n v \rangle$ is constant and one expects that

$$\Delta \nu \propto N_A .$$

For a saturated vapor, N_A is proportional to the vapor pressure, hence for a saturated vapor $\Delta\nu$ electron should track vapor pressure curves as a function of temperature. The special bulb results are plotted in figure 14, as are the vapor pressure curves of Ioli and Strumia[74] and those of Honig and Kramer.[75] This figure shows that the linewidth does indeed track the vapor pressure curve. The temperature for this run was measured using three copper constantan thermocouples which were cemented, one each, to the top, bottom, and middle of the cell with Corning heat sink cement. Prior to placing the cell in the oven, the oven was run to 500° C and held at that temperature for about 30 minutes. The oven then cooled to 140° C and the cell was inserted in the oven. This procedure of preheating the bricks greatly reduced the temperature gradients across the sample and also helped to stabilize the temperature. Typical temperature gradients across the sample were 5° C.

The linewidths measured at a given temperature are in excellent agreement with those of Balling[26] in which he used a bulb 60% coated with sodium. Other Na bulbs

FIGURE 14

ELECTRON LINEWIDTH VERSUS

Na VAPOR PRESSURE CURVES

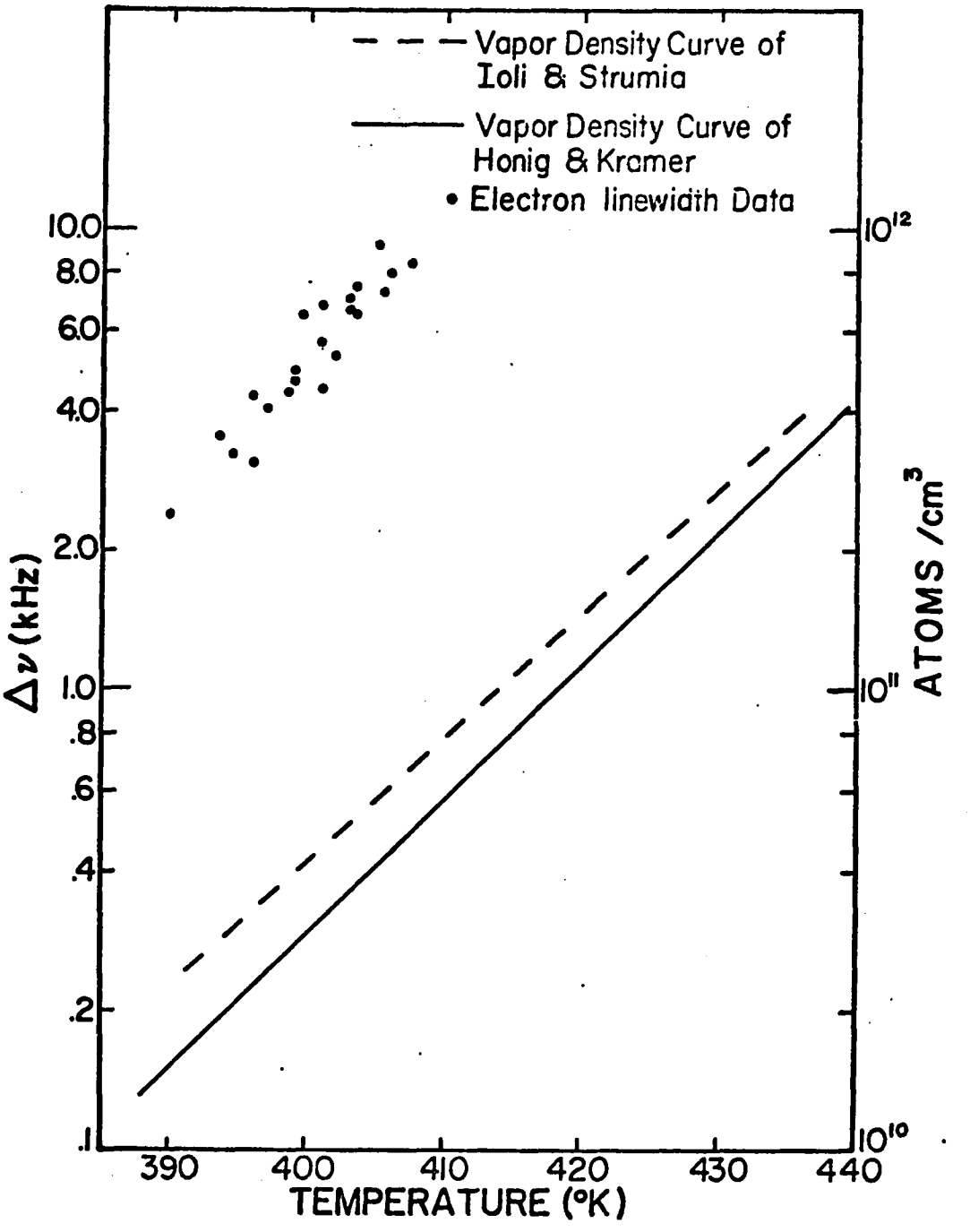
Vapor Density Curve of Ioli & Strumia
Vapor Density Curve of Honig & Kramer
• Electron linewidth Data
10.0
8.0
6.0
4.0
2.0
1.0
.8
.6
.4
.2
.1
Δν (kHz)
10^12
10^11
10^10
ATOMS /cm^3
390
400
410
420
430
440
TEMPERATURE (°K)

not well coated produced linewidths at a given temperature which were several times lower than those of the 75% coated sample. Ioli and Strumia[74] claim that cells 50% coated or better give saturated vapors. Also, by measuring Na signal amplitudes at a fixed temperature and under identical conditions, Balling[26] found no difference between the signal sizes in two bulbs, one 60% coated and the other 95% coated.

With all of the above results in mind it seems very unlikely that a factor of three error could exist in the linewidth measurements (which is what would be needed for these measurements to agree with Moores and Norcross[22, 23]) especially in view of the fact that even if the 75% coated bulb did not produce a saturated vapor, one would expect that the linewidth would be too narrow at a given temperature, not too wide.

The other comparison in table 4 is between the observed and predicted ratio

$$\frac{\left(\frac{\Delta\nu}{N_{Na}}\right)_{725^\circ K}}{\left(\frac{\Delta\nu}{N_{Na}}\right)_{403^\circ K}} .$$

The predicted ratio is about 8% higher than the upper limit of the present measurement.

The result that the spin-exchange cross section is constant over the temperature range measured is in contradiction to earlier results of this experiment.[76] The earlier conclusion that the electron linewidth did

not vary with temperature was drawn mainly from the results of a single quartz discharge sample. While measurements were being performed on this cell, the angle at which the white light beam fell on the entrance slits of the spectrometer was altered. As mentioned earlier, it was subsequently found that this can change the observed fractional absorption. The data from this cell is thus in strong suspect. The data from other samples run in the early phases of the experiment agree with the present results.

3. Comparison with Recent Experiments

It was also the intent of this experiment to check previous optical pumping results of e-Na and e-Rb spin-exchange collisions. Experimental results of Balling[26] for Na and those of Balling, Hanson, and Pipkin[24] for Rb are presented in table 5 along with those of the present experiment.

From table 5 we see that the agreement is quite good with the exception of the shift to linewidth ratio for Rb. BHP estimated a Rb polarization of $\sim 90\%$. The polarization measurements in the present experiment imply that the estimation of BHP was too high, a lower estimation would bring their results into good agreement with the present experiment.

4. Assignment of Errors

The errors quoted for $\frac{\Delta\nu}{N}\Big)_{T^\circ K}$ / $\frac{\Delta\nu}{N}\Big)_{\text{ROOM TEMP.}}$ for both the Na and Rb experiments represent the spread in the slopes for the total data taken for each alkali as stated at the beginning of this chapter. The errors for the electron linewidth measurements at 403°K for Na and 293°K for Rb appearing in table 4 are the maximum spreads in the data at those temperatures. The alkali atom density errors represent the uncertainty in the use of the vapor pressure curves of references 74 and 84, and were chosen to be 20%.

The errors assigned to the cross sections in table 5 are calculated by adding the $\Delta\nu$ and density errors in quadrature.

5. Conclusion

The linewidths at fixed alkali densities are in good agreement with previous experiments.[24, 26] There appears to be a real discrepancy between the results of the present experiment and the calculations of Moores and Norcross.[22,23] Because of the good agreement between their theory and experimental results in the eV range the lack of agreement here is difficult to understand, further investigation seems justified

Alkali Species	Buffer Gas	$\frac{\left(\frac{\Delta\nu}{N}\right)_{T°K}}{\left(\frac{\Delta\nu}{N}\right)_{\text{ROOM TEMP}}}$ (Room Temp=300°K for Rb; 400°K for Na)	$\frac{v_e \text{ (T °K)}}{v_e \text{ Room Temp}}$
Rb	14 Torr Ne	1.32 ± 0.15	1.46
Na	49 Torr Ne	1.45 ± 0.15	1.32

TABLE 1. Results of $\frac{\left(\frac{\Delta\nu}{N}\right)_{T°K}}{\left(\frac{\Delta\nu}{N}\right)_{\text{ROOM TEMP}}}$ for both e-Na and e-Rb collisions. T°K is 725°K for Na and 660°K for Rb.

Scattering Particles	σ_{se} (10^{-14} cm^2) at "Room Temp"
e-Rb	7.0 ± 2.0
e-Na	3.2 ± 1.0

TABLE 2. Measured values of e-Na and e-Rb spin exchange cross sections at "room temp.," (293°K for Rb and 403°K for Na).

Temperature °K	$\frac{2\delta\nu_0}{\Delta\nu}$	Polarization
190	.19 ± 0.05	.2 ± 0.1
300	.15 ± 0.01	.2 ± 0.1
600	0.055 ± 0.015	.1 ± 0.05

TABLE 3. Temperature dependence of $\frac{2\delta\nu_0}{\Delta\nu}$ for e-Rb collisions.

The quantity of theoretical interest is $\frac{2\delta\nu_0}{P(R)\,\Delta\nu}$.

	Experiment	Theory[22,23]	Experiment	Theory[22,23]
Na	$\frac{\Delta\nu}{N}(403°K) = \frac{(6.4\pm1.0)kH_z}{(5.0\pm1.0)\times10^{10}cm^{-3}} =$ $(1.3\pm0.3)\times10^{-7}\frac{cm^3}{sec}$	$\frac{\Delta\nu}{N}(403°K) =$ $0.45\times10^{-7}\frac{cm^3}{sec}$	$\frac{\Delta\nu/N(725°K)}{\Delta\nu/N(403°K)} =$ 1.45 ± 0.15	$\frac{\Delta\nu/N(725°K)}{\Delta\nu/N(403°K)} =$ 1.73
Rb	$\frac{\Delta\nu}{N}(293°K) = \frac{(1.3\pm0.2)\ kH_z}{(5.4\pm1.0)\times10^{9}\ cm^{-3}}$ $(2.4\pm0.6)\times10^{-7}\frac{cm^3}{sec}$		$\frac{\Delta\nu/N(660°K)}{\Delta\nu/N(300°K)} =$ 1.32 ± 0.15	

TABLE 4. Comparison of the measured temperature dependence of the electron linewidth at constant alkali density N for e-Na collisions to calculations of Moores and Norcross.[22,23] Rb-e results are also included. The density N was determined from recent vapor pressure measurements.[74,84]

Alkali Species	Temp. °K	$\Delta\nu$ (kHz)	$\frac{2\delta\nu_0}{\Delta\nu}$	Reference
Na	403	8.2 ± 2.0	$0.04 \leq (\frac{2\delta\nu_0}{\Delta\nu}) \leq .09$	26
Na	403	8.2 ± 1.0	———	This work
Rb	293	$1.3 \pm .1$	.042	24
Rb	293	$1.3 \pm .2$	$.15 \pm .01$	This work

TABLE 5. Comparison of present results to those of earlier experiments.[24,26]

BIBLIOGRAPHY

1. H. G. Dehmelt, Phys. Rev. 109, 381 (1958).

2. L. W. Anderson, F. M. Pipkin, J. C. Baird, Jr., Phys. Rev. Letters 4, 69 (1960).

3. L. W. Anderson, F. M. Pipkin, J. C. Baird, Jr., Phys. Rev. 120, 1279 (1960).

4. F. M. Pipkin and R. H. Lambert, Phys. Rev. 127, 787 (1962).

5. L. W. Anderson, F. M. Pipkin, and J. C. Baird, Jr., Phys. Rev. 116, 87 (1959).

6. R. H. Lambert and F. M. Pipkin, Phys. Rev. 128, 198 (1962).

7. R. E. Collins, B. Bederson, and M. G. Goldstein, Phys. Rev. 3, A1976 (1971).

8. D. M. Campbell, H. M. Brash, and P. S. Farago, Proc. Roy. Soc., to be published.

9. E. M. Purcell and G. B. Field, Astrophys. J. 124, 542 (1956).

10. P. R. Wesselius and I. Fejes, Astronomy and Astrophysics 24, 15 (1973).

11. R. A. Bernheim, Optical Pumping (Benjamin, New York, 1965).

12. P. L. Bender, Phys. Rev. 132, 2154 (1963).

13. F. Grossetete, Journal de Physique 25, 383 (1964).

14. H. A. Bethe and R. Jackiw, Intermediate Quantum Mechanics (W. A. Benjamin, New York, 1968) p. 206.

15. P. M. Stone and J. R. Reitz, Phys. Rev. 131, 2101 (1963).

16. J. C. Crown and A. Russek, Phys. Rev. 138, A 669 (1965).

17. L. C. Balling, Phys. Rev. 179, 78 (1969).

18. W. R. Garrett, Phys. Rev. 140, A 705 (1965).

19. P. Burke and H. M. Schey, Phys. Rev. 126, 147 (1962).

20. E. Karule, J. Phys. B. 5, 2051 (1972).

21. P. G. Burke and A. J. Taylor, J. Phys. B. 2, 869 (1969).

22. D. W. Norcross, J. Phys. B. 4, 1458 (1971).

23. D. L. Moores and D. W. Norcross, J. Phys. B. 5, 1482 (1972).

24. L. C. Balling, R. J. Hanson, and F. M. Pipkin, Phys. Rev. 133, A 607 (1964).

25. L. C. Balling and F. M. Pipkin, Phys. Rev. 136, A 46 (1964).

26. L. C. Balling, Phys. Rev. 151, 1 (1964).

27. P. L. Bender, Phys. Rev. 134, A 1174 (1964).

28. L. C. Balling, R. H. Lambert, J. J. Wright, and R. E. Weiss, Phys. Rev. Letters 22, 61 (1969).

29. J. J. Wright, L. C. Balling, and R. H. Lambert, Phys. Rev. A 4, 1018 (1970).

30. R. E. Weiss, R. H. Lambert, and L. C. Balling, Phys. Rev. 2, 1745 (1970).

31. S. J. Davis, J. J. Wright, and L. C. Balling, Phys. Rev. 3, A 1220 (1971).

32. G. Herzberg, Atomic Spectra and Atomic Structure, (Dover Publications, New York, 1945) 2nd Edition.

33. R. B. Leighton, Principles of Modern Physics, (McGraw-Hill, New York, 1959).

34. M.I.T. Wavelength Tables (M.I.T. Press, Cambridge, Massachusetts, 1969).

35. R. A. Bernheim, Optical Pumping, (W. A. Benjamin, New York, 1965). p. 6.

36. R. L. deZafra, Am. J. Phys. 28, 646 (1960).

37. A. Gallagher, Phys. Rev. 157, 68 (1967); 163, 206 (1967).

38. S. M. Jarrett, Phys. Rev. 133, A 111 (1964).

39. H. G. Dehmelt, Phys. Rev. 105, 1487 (1957).

40. W. Franzen and A. G. Emslie, Phys. Rev. 108, 1453 (1957).

41. W. Happer, Reviews of Modern Physics 44, 169 (1972).

42. C. P. Slichter, Principles of Magnetic Resonance, (Harper and Row, New York, 1963). p. 11.

43. T. R. Carver, Science 141, 599 (1963).

44. J. P. Wittke and R. H. Dicke, Phys. Rev. 103, 620 (1956).

45. A. Dalgarno, Proc. Roy. Soc. (London) A 262, 132 (1961).

46. A. E. Glassgold, Office of Naval Research, Technical Report N 65-1 (1964).

47. E. Merzbacher, Quantum Mechanics (John Wiley and Sons, New York, 1970).

48. S. DeBenedetti, Nuclear Interactions (John Wiley and Sons, New York, 1964).

49. C. P. Slichter, Principles of Magnetic Resonance (Harper and Row, New York, 1963). p. 28.

50. F. Bloch and A. Siegert, Phys. Rev. 70, 460 (1946).

51. U. Fano, Rev. Mod. Phys. 29, 74 (1957).

52. G. V. Skrotskii and T. G. Izyumova, Soviet Phys. Usp. 4, 177 (1961).

53. S. Penselin, T. Moran, and V. W. Cohen, Phys. Rev. 127, 524 (1962).

54. S. B. Crampton, Phys. Rev. 3A, 515 (1971).

55. H. Gibbs, Phys. Rev. 139, A 1374 (1965).

56. H. M. Gibbs, Phys. Rev. 3A, 500 (1971).

57. R. H. Lambert, Phys. Rev. A 1, 1841 (1970).

58. H. A. Bethe and R. Jackiw, Intermediate Quantum Mechanics (W. A. Benjamin, New York, 1968). p. 227.

59. R. H. Dicke, Phys. Rev. 89, 472 (1953).

60. A. Abragam, Principles of Nuclear Magnetism, (Clarendon Press, Oxford, 1961), p. 424.

61. Buffer Gases purchased from Cryogenics-East, Inc., 128 Wheeler Road, Burlington, Massachusetts, Distributors for Linde Specialty Gas.

62. F. A. Jenkins and H. E. White, Fundamentals of Optics (McGraw Hill, New York, 1957) 3rd Edition, p. 529.

63. S. Dushman, Scientific Foundations of Vacuum Technique (John Wiley and SOns, New York, 1949).

64. T. R. Carver, F. R. Lewis, Jr., R. E. Pollack, and G. E. Schrank, Rev. Sci. Instr. 32, 861 (1961).

65. A. C. G. Mitchell and M. W. Zemansky, Resonance Radiation and Excited Atoms (MacMillan, Cambridge, England, 1934) p. 21.

66. Fiberfrax insulation, Carborundum Company, Refractories Division, Box 337, Niagara Falls, New York.

67. R. J. Hanson and F. M. Pipkin, Rev. Sci. Instr. 36, 179 (1965).

68. Firebrick Type Jm-23, Refractories and Building Specialties, Inc., 767 Concord Avenue, Cambridge, Massachusetts.

69. R. E. Weiss, Ph.D. Thesis, Dept. of Physics, University of New Hampshire, 1969.

70. A. C. G. Mitchell and M. W. Zemansky, Resonance Radiation and Excited Atoms (MacMillan, Cambridge, England, 1934) Chapt. 4.

71. H. W. Thompson, Advances in Spectroscopy (Interscience, New York, 1961) Vol. II, p. 6.

72. N. Ioli and F. Strumia, Proceedings of the International Conference on Optical Pumping and Atomic Lineshape, (Warsaw, Poland, 1968).

73. Tritium gas, purchased from Oak Ridge National Laboratory, Oak Ridge, Tennessee.

74. N. Ioli, F. Strumia, and A. Moretti, J. Opt. Soc. Am. 61, 1251 (1971).

75. R. E. Honig and D. A. Kramer, R.C.A. Review, 1969, p. 285 (unpublished).

76. S. J. Davis and L. C. Balling, Phys. Rev. 6A, 1479 (1972).

77. J. P. Barrat, Proc. Roy. Soc. (London) A 263, 371 (1961).

78. J. P. Barrat and C. Cohen-Tannoudji, Compt. Rend. 252, 93, 255 (1961).

79. C. Cohen-Tannoudji, Ann. Phys. (Paris) 7, 423, 469 (1962).

80. B. Bederson and W. Fite, Methods of Experimental Physics (Academic Press, New York, 1968) Vol. 7, p. 143.

81. G. K. Woodgate and J. S. Martin, Proc. Phys. Soc. (London) 70, 485 (1957).

82. L. Evans, P. G. H. Sanders, G. K. Woodgate, Proc. Roy. Soc. (London) 289A, 108 (1965).

83. C. Schwartz, Phys. Rev. 97, 380 (1955).

84. E. L. Lewis and A. Gallagher, J. Opt. Soc. Am. (to be published).

APPENDIX I

SPIN-FLIP CROSS SECTION

The form of the spin-exchange cross section for two spin 1/2 particles is calculated from elementary scattering theory. We assume the system to be composed of 2 spin 1/2 particles: 1 and 2. Neglecting spin, one usually writes the asymptotic solution as the sum of an incident plane wave and an outgoing spherical wave,

$$\psi \sim \left[e^{ikz} + \frac{f(\theta)\, e^{ikr}}{r} \right],$$

where the incident wave is assumed incident along the z axis and f (θ) is the scattering amplitude. If the scattering is spin dependent then of course spin terms must be included.

For two spin 1/2 particles there are four possible spin states:

$$\chi_3^1 = \alpha_1 \alpha_2,$$

$$\chi_3^0 = \frac{1}{\sqrt{2}} \left[\alpha_1 \beta_2 + \beta_1 \alpha_2 \right],$$

$$\chi_3^{-1} = \beta_1 \beta_2,$$

$$\chi_1^0 = \frac{1}{\sqrt{2}} \left[\alpha_1 \beta_2 - \beta_1 \alpha_2 \right],$$

where α and β represent the spin up and down states respectively. To include spin effects the scattering amplitude is rewritten[48]

$$M(\theta) = P_1 f_1(\theta) + P_3 f_3(\theta).$$

Only singlet and triplet states are present. P_1 and P_3 are the singlet and triplet projection operators.

If the initial spin state is $|i\rangle$ then the final scattered wave is

$$\psi_f = \left[e^{ikz} + \frac{e^{ikr}}{r} M(\theta) \right] |i\rangle$$

The amplitude to scatter from some initial spin state $|i\rangle$ to some final spin state $|f\rangle$ is given by $\langle f|M(\theta)|i\rangle$ We want the amplitude to go from an initial state $|\alpha_1\beta_2\rangle$ to a final state $|\beta_1\alpha_2\rangle$.

So

$$\langle \beta_1\alpha_2 | M(\theta) | \alpha_1\beta_2 \rangle$$

$$= \langle \beta_1\alpha_2 | P_1 f_1(\theta) + P_3 f_3(\theta) | \alpha_1\beta_2 \rangle .$$

Solving for $\alpha_1\beta_2$ and $\beta_1\alpha_2$ in terms of triplet and singlet states leads to

$$\left\langle \frac{1}{\sqrt{2}}(\chi_3^0 - \chi_1^0) \right| P_1 f_1(\theta) + P_3 f_3(\theta) \left| \frac{1}{\sqrt{2}}(\chi_3^0 + \chi_1^0) \right\rangle = \frac{1}{2}\left[f_3(\theta) - f_1(\theta) \right] .$$

This is the differential scattering amplitude, so the differential cross section is

$$\frac{d\sigma_{se}}{d\Omega} = \frac{1}{4} \left| f_3(\theta) - f_1(\theta) \right|^2 .$$

Therefore, the total spin-exchange cross section is

$$\sigma_{se} = \frac{1}{4} \int \left| f_3(\theta) - f_1(\theta) \right|^2 d\Omega .$$

APPENDIX II

PUMPING EQUATION

Many papers have appeared describing the optical pumping process via the density matrix.[77,78,79] The following, utilizing the density matrix, outlines steps that lead to the pumping equation for a fictitious nuclear spin zero alkali atom.

Under the effect of left circularly polarized pumping light, the rate equations for the diagonal density matrix elements, assuming complete reorientation in the excited state, are[24]

$$\dot{\rho}_{11}(A) = \frac{1}{2}\int_0^\infty I(\nu,z)\,\sigma(\nu)\,\rho_{zz}(A,z)\,d\nu ,$$

and

$$\dot{\rho}_{zz}(A) = -\frac{1}{2}\int_0^\infty I(\nu,z)\,\sigma(\nu)\,\rho_{zz}(A,z)\,d\nu ,$$

where $\sigma(\nu)$ is the absorption cross section for unpolarized atoms. The factor of $\frac{1}{2}$ accounts for the fact that if complete reorientation takes place in the excited state then there is a probability of $\frac{1}{2}$ that the atom will fluoresce back to the lower ground state from which it was pumped. This cycle leaves the relative ground state populations unchanged. The factor of $\frac{1}{2}$ does not appear in ref. 24 because their " $\sigma(\nu)$ " is twice the corresponding term here.

Using

$$\dot{P}(A) = \dot{\rho}_{\perp}(A) - \dot{\rho}_{zz}(A) ,$$

we get

$$\dot{P}(A) = \int_0^\infty I(\nu, z)\, \sigma(\nu)\, \rho_{zz}(A, z)\, d\nu .$$

In appendix III it is shown that

$$I(\nu, z) = I(\nu, 0)\, e^{-\int_0^z N_A\, \sigma(\nu)\, \rho_{zz}(A, \zeta)\, d\zeta} .$$

So we have

$$\dot{P}(A) = \int_0^\infty I(\nu,0)\, \sigma(\nu)\, \rho_{zz}(A, z)\, e^{-\int_0^z N_A\, \sigma(\nu)\, \rho_{zz}(A,\zeta)\, d\zeta}\, d\nu .$$

If we now take the Z average over the length of the cell Z_0 we obtain

$$\langle \dot{P}(A) \rangle = \frac{1}{Z_0} \int_0^{Z_0} dz \int_0^\infty I(\nu,0)\, \sigma(\nu)\, \rho_{zz}(A, z)\, e^{-\int_0^z N_A\, \sigma(\nu)\, \rho_{zz}(A,\zeta)\, d\zeta}\, d\nu ,$$

$$= \frac{1}{Z_0} \int_0^{Z_0} dz \int_0^\infty I(\nu,0)\, \frac{d}{dz} \left[\int_0^z \sigma(\nu)\, \rho_{zz}(A,\zeta)\, d\zeta \right] e^{-\int_0^z N_A\, \sigma(\nu)\, \rho_{zz}(A,\zeta)\, d\zeta}\, d\nu ,$$

where the fact that

$$\frac{d}{dx} \int_0^X f(x)\, dx = f(X)$$

has been used.

Performing the integral gives

$$\langle \dot{P}(A) \rangle = \frac{1}{N_A z_0} \int_0^\infty d\nu \; I(\nu,0) \left(1 - e^{-z_0 \sigma(\nu) \langle \rho_{22}(A) \rangle N_A}\right).$$

In the limit of low absorption this can be written

$$\langle \dot{P}(A) \rangle \approx \frac{1}{N_A z_0} \int_0^\infty d\nu \; I(\nu,0) \left[1 - 1 + z_0 \sigma(\nu) \langle \rho_{22}(A) \rangle N_A\right].$$

So

$$\frac{d\langle P(A) \rangle}{dt} = \langle \rho_{22}(A) \rangle \int_0^\infty I(\nu,0) \sigma(\nu) \, d\nu .$$

Observing that

$$\langle \rho_{22}(A) \rangle = \frac{1 - \langle P(A) \rangle}{2} ,$$

yields

$$\frac{d\langle P(A) \rangle}{dt} = \left[1 - \langle P(A) \rangle\right] \frac{1}{2} \int_0^\infty I(\nu,0) \sigma(\nu) \, d\nu .$$

We now define the pumping rate as

$$\frac{1}{T_p} = \frac{1}{2} \int_0^\infty I(\nu,0) \sigma(\nu) \, d\nu .$$

Thus

$$\frac{d\langle P(A) \rangle}{dt} = \frac{1}{T_p} - \frac{\langle P(A) \rangle}{T_p} .$$

APPENDIX III

THE OPTICAL PUMPING SIGNAL

The intensity of radiation of frequency ν absorbed by a thin layer ∂z of absorbing material of density N is given by Lambert's law[80]

$$\partial I(\nu, z) = - I(\nu, z)\, \sigma(\nu)\, N\, \partial z ,$$

where $\sigma(\nu)$ is the absorption cross section. For the case of the incident light being left circularly polarized, alkali pumping radiation incident on a cell of length Z_o containing the same alkali vapor in a weak axial magnetic field, not all atoms can absorb the light. For a fictitious spin $\frac{1}{2}$ alkali only those in the state $m_F = -\frac{1}{2}$ can absorb. The probability to be in the $m_F = -\frac{1}{2}$ state is $\rho_{22}(A)$. So the expression becomes

$$\partial I(\nu, z) = - I(\nu, z)\, \sigma(\nu)\, N_A\, \rho_{22}(A)\, \partial z .$$

Integrating this over the length of the cell Z_o gives

$$\ln I(\nu, z_o) - \ln I(\nu, 0) = - \int_0^{z_o} \sigma(\nu) N_A\, \rho_{22}(A)\, dz$$

or

$$I(\nu, z_o) = I(\nu, 0)\, e^{- \int_0^{z_o} \sigma(\nu) N_A\, \rho_{22}(A, z)\, dz} ,$$

where $I(\nu, Z_0)$ is the transmitted light intensity of frequency ν, and $I(\nu, o)$ is the incident light intensity. But since the Z average of a function $g(z)$ is given by

$$g = \frac{1}{Z_0} \int_0^{Z_0} g(z)\, dz ,$$

we get

$$I(\nu, Z_0) = I(\nu, 0)\, e^{- Z_0 \sigma(\nu) N_A \langle \rho_{zz}(A) \rangle} .$$

The total transmitted light intensity is found by integrating over the frequencies,

$$I = \int_0^{\infty} I(\nu, 0)\, e^{- Z_0 \sigma(\nu) N_A \langle \rho_{zz}(A) \rangle}\, d\nu .$$

In the low light absorption limit,

$$I \approx \int_0^{\infty} I(\nu, 0) \left[1 - Z_0 \sigma(\nu) N_A \langle \rho_{zz}(A) \rangle \right] d\nu .$$

Using

$$\langle \rho_{zz}(A) \rangle = \frac{1}{2} \left(1 - \langle P(A) \rangle \right),$$

one gets

$$I = \int_0^{\infty} I(\nu, 0) \left[1 - \frac{1}{2} \left(1 - \langle P(A) \rangle \right) Z_0 \sigma(\nu) N_A \right] d\nu .$$

The observed optical pumping signal is proportional to the difference δI in the transmitted light intensity between the two cases rf off and rf on,

$$\delta I = \int_0^{\infty} I(\nu, 0)\, Z_0 N_A \sigma(\nu) \frac{\langle \delta P(A) \rangle}{2}\, d\nu .$$

Defining the pumping rate as in appendix II,

$$\frac{1}{T_p} = \frac{1}{2}\int_0^\infty I(\nu,0)\,\sigma(\nu)\,d\nu,$$

one gets

$$\delta I = \frac{Z_0 N_A}{T_p} \langle \delta P(A) \rangle$$

This represents the change in intensity δI . The actual observed optical pumping signal however, is represented by the corresponding change in the total light energy δI_T , or

$$\delta I_T = \frac{Z_0 N_A A}{T_p} \langle \delta P(A) \rangle ,$$

where A is the cross sectional area of the cell.

APPENDIX IV

GROUND STATE HYPERFINE STRUCTURE OF Mn^{55}

1. Introduction

Prior to the experiment just described, the ground state hyperfine structure of Mn^{55} was measured in a spin-exchange optical pumping experiment. The details of this work are reported in ref. 31. The intention here is to give a brief description of the experiment and the results to stress the utility of both spin-exchange and high temperature optical pumping.

The hyperfine structure of the $S_{\frac{5}{2}}$ ground state ($I = \frac{5}{2}$, $J = \frac{5}{2}$) had been previously investigated by atomic beam workers.[81,82] There are five hyperfine transition frequencies from which one can determine five multipole interaction constants in the Hamiltonian. First order perturbation theory relates these constants to electric and magnetic multipole interactions for atoms where coupling is a good approximation. In many cases, however, relativistic effects, configuration mixing, and higher order perturbation terms contribute significantly to the interaction constants. In this case, measurements of the interaction constants can lead to a refinement of theoretical wave functions.

In the most recent atomic-beam experiment, three

hyperfine frequencies were measured to determine the magnetic dipole and electric quadrupole interaction constants A and B. The value of B was attributed to relativistic effects. The three remaining interaction constants were set equal to zero.

2. Apparatus

A block diagram of the apparatus is shown in figure 15. With the exception of no white light side holes in the shields, the Mn apparatus was almost identical to that of the Rb and Na experiments just described. The cells were 300 ml quartz spheres. The rf was derived by frequency multiplying the output of the GR Frequency Synthesizer by means of a varactor diode circuit.

3. Measurements

The measurements were carried out in a low (4 mG) field so that all the Zeeman splittings were equal. The hyperfine transition frequencies are related to the multipole moments through the equations,[83]

$$\nu(F=5 \leftrightarrow F=4) = 5A + \tfrac{3}{5}B + \tfrac{24}{5}C + 8D + 12E,$$

$$\nu(F=4 \leftrightarrow F=3) = 4A - \tfrac{3}{50}B - \tfrac{174}{25}C - 26D - 66E,$$

$$\nu(F=3 \leftrightarrow F=2) = 3A - \tfrac{9}{25}B - \tfrac{8}{25}C + 40D + 220E,$$

$$\nu(F=2 \leftrightarrow F=1) = 2A - \tfrac{39}{100}B + \tfrac{153}{25}C - 15D - 495E,$$

$$\nu(F=1 \leftrightarrow F=0) = A - \tfrac{6}{25}B + \tfrac{144}{25}C - 48D + 792E.$$

FIGURE 15

BLOCK DIAGRAM OF Mn APPARATUS

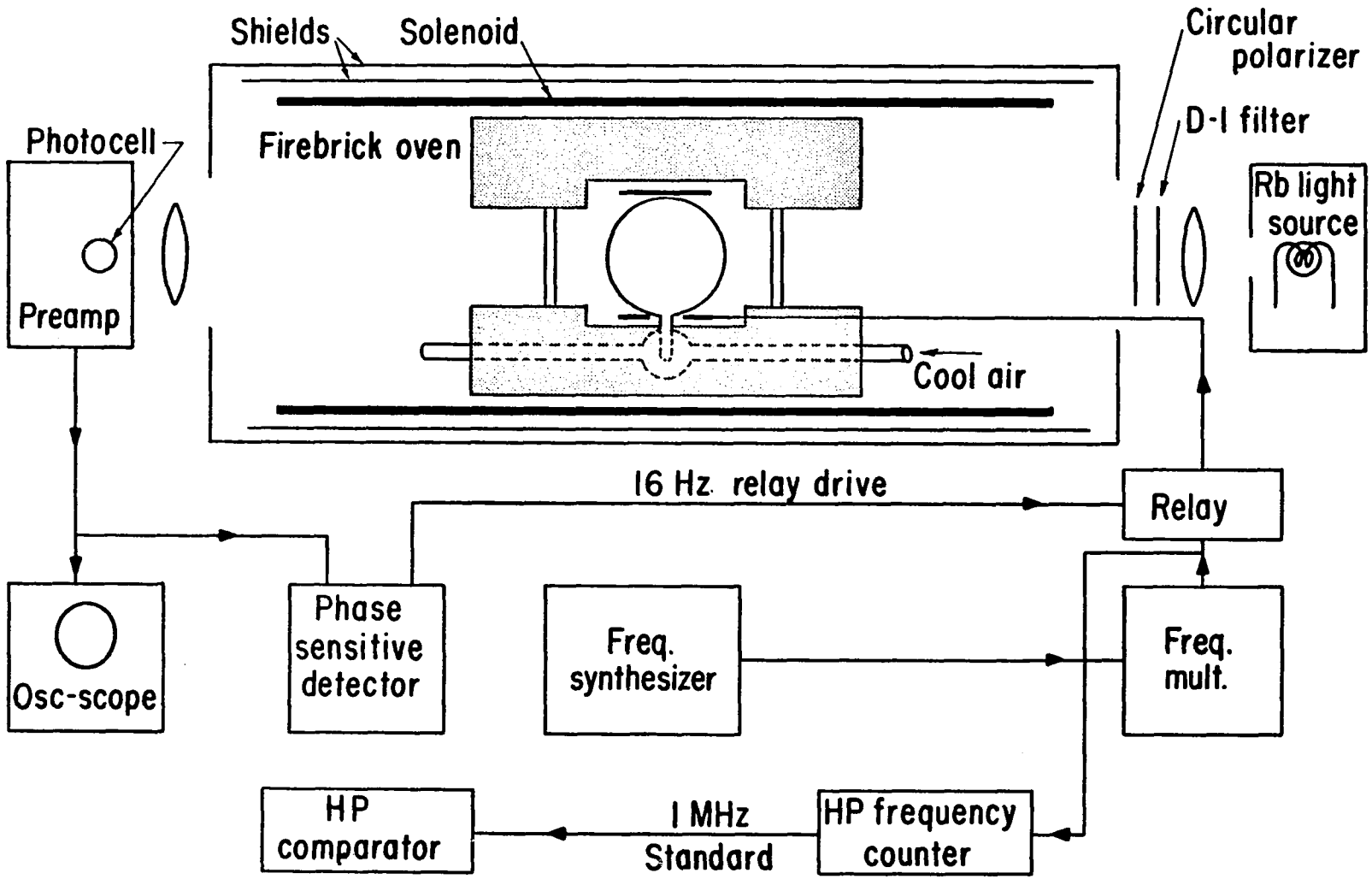
Shields
Solenoid
Circular polarizer
D-I filter
Photocell
Firebrick oven
Rb light source
Preamp
Cool air
16 Hz relay drive
Relay
Osc-scope
Phase sensitive detector
Freq. synthesizer
Freq. mult.
HP comparator
1 MHz Standard
HP frequency counter

where A, B, C, D, and E are the $2^{\underline{1}}$, $2^{\underline{2}}$, $2^{\underline{3}}$, $2^{\underline{4}}$, $2^{\underline{5}}$ pole interaction constants respectively. The signals were very weak and only on one sample was it possible to measure all five transition frequencies. Three and sometimes four transition frequencies were measured on other cells. All measurements were performed at 725°C.

4. Results

The results are detailed in tables I-IV of ref. 31. Only the final results are quoted here. A was found to vary linearly with neon pressure and the fractional pressure shift was determined to be

$$\frac{1}{A}\left(\frac{\partial A}{\partial P}\right) = (2.6 \pm 0.2) \times 10^{-8}\ \text{Torr}^{-1}\ .$$

The zero pressure intercept gave A = -72420836 (15) Hz.

No pressure dependence was observed for B and C. The quoted values of the other 4 interaction constants are

$$B = -19031\ (17)\ \text{Hz},$$

$$C = -0.7 \pm 1.1\ \text{Hz},$$

$$|D| < 0.25\ \text{Hz},$$

$$|E| < 0.02\ \text{Hz}.$$

The zero pressure A is in excellent agreement with the latest atomic beam value as is B. B also is in good agreement with the latest calculation. The small values of C, D, and E justify their being set equal to zero in the less precise atomic beam experiment.[81,82]